Let Them Fall Where They May:
Capture Regions of Curved Objects and Polyhedra

David J. Kriegman
Center for Systems Science
Departments of Electrical Engineering and Computer Science
Yale University
New Haven, CT 06520-8267
USA
kriegman@cs.yale.edu
(203) 432-4091
FAX: (203) 432-7481

September 24, 1997

Abstract

When a three dimensional object is placed in contact with a supporting plane, gravitational forces move it to one of a finite set of stable poses. For each stable pose, there is a region in the part's configuration space called a capture region; for any initial configuration within the region, the object is guaranteed to converge to that pose. The problem of computing maximal capture regions from an object model is analyzed assuming only that the dynamics are dissipative; the precise equations governing the system are unnecessary. An algorithm, based on Morse theory, is first developed for objects with smooth convex hulls. The formulation is then extended to objects with piecewise-smooth hulls using a catalogue of critical points derived from stratified Morse theory. Algorithms have been fully implemented for objects with smooth and polyhedral convex hulls. As examples from the implementation demonstrate, calculating these regions from a geometric model is computationally practical.

1

1 Introduction

Actions have consequences; automatic planning, that is determining a sequence of actions in order to accomplish a task, is only possible if the consequences can be predicted. In this paper, a prediction problem is considered which has useful application in automatic robot planning and the design of parts feeders. When an object statically rests on a supporting plane such as a tabletop or conveyer belt, it generally assumes one of a finite set of stable configurations.[1] Simply knowing the stable poses (also called natural resting aspects (Boothroyd, Redford, Poli & Murch 1972)) is useful for many tasks in robotic and manufacturing applications, e.g., it may aid sensing decisions, grasp planning, and reorienting maneuvers (Lozano-Perez, Jones, Mazer & O'Donnell 1992; Murase & Nayar 1994; Rao, Kriegman & Goldberg 1995; Tournassoud, Lozano-Perez & Mazer 1987).

While the configuration space, *C-space*, of a rigid object is generally six dimensional, it can be treated as a two dimensional sphere for the problem considered here. If an accurate and complete model of the object's dynamics were known, the sphere could be partitioned into a collection of open sets called *capture regions* (basins of attraction, stability regions, regions of convergence) (Chiang, Hirsch & Wu 1988; Genesio, Tartaglia & Vicino 1985). Starting at rest from any point in a capture region, the object's pose will converge under the force of gravity to the corresponding stable configuration.

Let us consider the application of capture regions in a parts feeding system. Objects enter a feeder in an arbitrary pose, and the feeder reorients them so they emerge in the same pose. See (Carlisle, Goldberg, Rao & Wiegley 1994) for a recent overview. When the capture region of the desired stable pose is known, the feeder is only required to reorient a part to a configuration within that region. Gravity will do the rest. Based on the capture regions of a part and a set of actions that a mechanism can perform, a transition graph can be constructed in which the nodes correspond to the stable configurations of the part. A directed arc exists between two nodes if there is a non-empty set of actions that move the part from the stable configuration of the source node to a configuration within the capture region of the destination node. For a part with n stable configurations, the size of the graph is $O(n^2)$. A path through this transition graph constitutes a plan to move a part between two arbitrary stable configurations. Algorithms for constructing the transition graph are presented in (Rao et al. 1995) for feeding polyhedral parts with a passive pivoting gripper, and the use of capture regions in this application are discussed in Section 6. The capture regions can be likened to the backprojections found in the work of (Lozano-Pérez, Mason & Taylor 1982), (Erdmann 1986), and (Donald 1988). (Erdmann, Mason & Vaneček 1993) describe a related planner for polyhedral parts on a tilting table.

As mentioned above, if the object's dynamics were accurately known (and time invariant and deterministic, etc.), then it would be possible to completely partition the *C-space* using the methods presented in (Brost 1992; Chiang et al. 1988). Unfortunately, while some aspects of the dynamics can be modeled and certain parameters (e.g. mass and inertia) can be measured, it is impractical to completely model other effects such as rolling and sliding friction, bouncing, air viscosity, etc. In situations where a part is sliding on a surface or a 3-D object is moving through a viscous medium, the quasi-static approximation can be applied (Peshkin & Sanderson 1989); however, this is unreasonable for an object rolling or tumbling on a table under the influence of gravity. Instead,

---

[1]Exceptions include objects with cylindrical or spherical sections where the center of gravity is located at the geometric center.

we only assume that the object starts at rest and that the dynamics are dissipative (i.e. nothing adds energy to the system); there may be rolling and slipping. Because of these weak assumptions about the dynamics, the ultimate stable pose cannot be determined for all initial configurations, and so the set of capture regions does not completely cover the *C-space*.

(Boothroyd et al. 1972; Boothroyd & Ho 1977) considered the related problem of computing the statistical distribution of stable poses for a few simple shapes. (Ngoi, Lim & Lee 1995) proposed a heuristic algorithm for computing the distribution by calculating the solid angle of a face from the centroid; they compared the predicted distribution to ones found experimentally. Note that when the prior distribution of initial configurations is known the presented approach can be used to compute a lower bound on the probability of a part resting in each stable pose since the capture regions do not completely cover the sphere. (Wiegley, Rao & Goldberg 1992) consider the problem of computing capture regions of polyhedra assuming a quasi-static model of object motion. (Brost 1991*a*; Brost 1992) presents a method for partitioning the configuration space ($\mathbb{R}^2 \times S^1$) for a variety of planar manipulation tasks (e.g. pushing, part fixturing and grasping) involving polygons moving in the plane. Similar energy arguments were applied to determine "puddles" in the configuration space. (Brost 1992) also considered the problem when the dynamics were fully specified and when there was a limited amount of parametric uncertainty. This paper extends work in (Kriegman 1992) which presented an implemented algorithm for determining stable poses (but not capture regions) of piecewise-smooth objects. Except for preliminary results for smooth surfaces presented in (Kriegman 1994), computation of capture regions has not been considered for 3-D objects.

In the next section the relationship between dissipative dynamics and capture regions are considered; we then show that the configuration space of an object in contact with a supporting plane is equivalent to a sphere. Simple objects with a smooth (up to third order) convex hull are first addressed, and the problem of computing capture regions can be solved by applying Morse theory. An algorithm has been implemented for computing the capture regions for a part whose convex hull is modelled by an algebraic surface, and a few examples are presented. After having established the essence of the approach for smooth surfaces, objects with piecewise-smooth convex hulls are considered using stratified Morse theory. An algorithm has been implemented for polyhedra, and results from the implementation are discussed. We conclude by discussing the application of these results to a particular parts feeding paradigm and some other possible future directions.

2 Dissipative Dynamics

For a mechanical system with totally dissipative dynamics, the total mechanical energy E along any trajectory is always decreasing. If $\mathbf{q}$ denotes the configuration of the system, then a system is totally dissipative if $\dot{E}(\mathbf{q}(t)) < 0$ for $\dot{\mathbf{q}} \neq \mathbf{0}$. While kinetic and potential energy may be traded off at different points in the state space, no energy is added to the system; instead phenomena such as friction and viscoelasticity cause a continual loss of mechanical energy as time evolves. While the study of such systems dates to the development of the theory of classical mechanics, this work is strongly motivated by Koditschek's results for robotics applications such as adaptive control and motion planning using artificial potential fields (Koditschek 1991; Rimon & Koditschek 1992). In particular, it was noted that a potential energy function can be defined on the space of mechanism configurations, and that the only stable attractors of a totally dissipative system correspond to local minima of the potential energy function. Because the total energy is strictly decreasing over
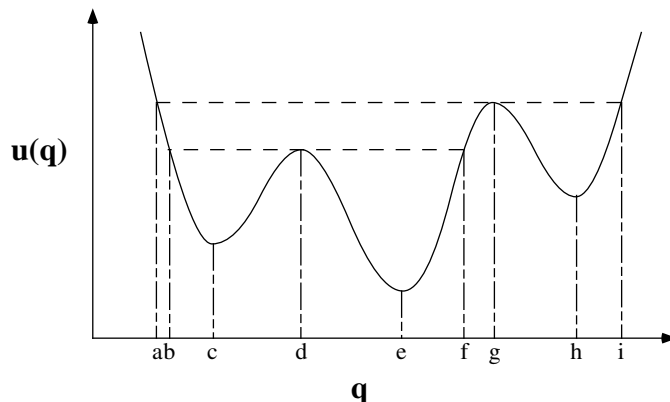
Figure 1: The potential energy $u(q)$ for a dynamical system with one degree of freedom q.

time, such a system does not have any limit cycles.

In the application considered here, the potential energy of an object under gravity can be expressed as a function of its location with respect to the supporting plane; the local minima of this function correspond to the stable poses. To illustrate the essential ideas, consider a simplified example in Figure 1 of the graph of potential energy $u(q)$ for a dissipative system with one degree of freedom q. There are three local minima (configurations c, e, and h). The question arises, if the system starts at rest in some other configuration $q(t_0) = q_0$ besides c, e or h, then which one will it converge to? Assuming that the system starts at rest $\dot{q}(t_0) = 0$, the total energy will simply be the potential energy $u(q_0)$. Furthermore, since the system is dissipative, the total energy will never exceed $u(q_0)$. For the system illustrated in Figure 1, consider the open interval (b, d). Since d is a local maximum of $u(q)$ and $u(b) = u(d)$, $\forall q \in (b, d), u(q) < u(d)$. Because there is only one minimum c in the interval, the interval (b, d) is a *capture region* for stable configuration c. Furthermore, (b, d) is that largest (maximal) region that is guaranteed to converge to c, and this can be seen by considering the consequences of expanding the interval. If the interval were expanded to (b, d^*) where $d < d^* < f$, then for an initial configuration in $q(t_0) \in (d, d^*)$, the system would converge to e. Alternatively, if the interval were expanded to (b^*, d) where $b^* < b$, then there exists a dissipative system such that the system would converge to e and not c for some $q_0 \in (b*, b)$. Similarly (d, f) and (g, i) are respectively capture regions for e and h. Note that we have not made any strong assumptions about the system's dynamics; the precise form of the governing differential equations does not need to be known. This observation was also exploited in (Brost 1991a; Brost 1992).

So what can be concluded about an initial configuration in the other intervals $(-\infty, b]$, $[f, g]$, $[i, \infty)$? Unfortunately, without additional knowledge (or assumptions) about the actual dynamics, only weaker predictions are possible. By the same energy argument, for any $q(t_0) \in (a, g)$, the system will not converge to h, but it will converge to either c or e though we cannot determine which one. Note that $(b, d) \subset (a, g)$ and $(d, f) \subset (a, g)$. These relationships define a tree representing the containment or hierarchy of capture regions, and this tree may also be useful for planning.

3 Configuration Space and Convex Hulls

To determine the maximal capture regions of a 3-D object (a bounded, compact set) and a supporting plane, we will subsequently consider its configuration space *C-space* and define a potential energy function on the *C-space*. Following (Latombe 1991), we note that the *C-space* of a rigid body is equivalent to $\mathbb{R}^3 \times SO(3)$. It can be expressed as the union of two disjoint sets: *C-free* where the object does not intersect the plane, and *C-obstacle* where the object and plane intersect. *C-obstacle* is a closed set, and its boundary, denoted by *C-contact*, is the set of configurations where the part just touches the plane.

Note that an object only contacts a plane on its convex hull $\mathcal{H}$ since the hull can be defined by the set of planes which envelop the object. Thus, the partitioning of *C-space* into *C-free*$\cup$ *C-obstacle* generated by an object and its hull are identical; so, it is only necessary to consider computing capture regions of convex objects. When computing capture regions of a nonconvex part, its hull can be computed first. In general, the convex hull of a nonconvex object is piecewise-smooth; even for a smooth surface with concavities, the hull is only $\mathcal{C}^1$. Initially, we are going to be more restrictive and assume that the surface of the hull is at least thrice differentiable $\mathcal{C}^3$ allowing us to apply Morse theory in Section 4. These results will be generalized to parts whose hulls are not smooth in Section 5.

The potential energy of an object is proportional to the height of the center of gravity above the horizontal support plane. In turn, the location of the center is a function of the part's configuration $\mathbf{q}$. Now, consider a fixed coordinate system whose origin lies in the supporting plane, and let the coordinates of the gravity vector $\mathbf{g}$ be $[0\ 0\ 1]^t$ in this frame. Let $\mathbf{c}$ denote the coordinates of the center of gravity in a frame affixed to the moving part. The configuration $\mathbf{q} = (\mathbf{t}, \mathbf{R}) \in \mathbb{R}^3 \times SO(3)$ of the part with respect to the fixed frame can be represented by $\mathbf{t} = [t_x\ t_y\ t_z]^t$ and $\mathbf{R} = [\mathbf{r}_1|\mathbf{r}_2|\mathbf{r}_3]^t$. Assuming unit mass and taking the potential to be 0 when the center lies in the support plane, the potential energy can be written as:

$$u(\mathbf{q}) = (\mathbf{R}\mathbf{c} + \mathbf{t}) \cdot \mathbf{g} = \mathbf{r}_3 \cdot \mathbf{c} + t_z \tag{1}$$

Thus, the potential energy is a function of only $\mathbf{r}_3$ and t_z. Since $\mathbf{R}$ is an orthonormal matrix, $|\mathbf{r}_3| = 1$; in other words $\mathbf{r}_3$ lies on the two sphere S^2. Rotation about $\mathbf{g}$ and translation in a direction parallel to the support plane leaves $u(\mathbf{q})$ unchanged. Furthermore, the components of $\mathbf{q}$ specifying the resting location and orientation in the support plane cannot be predicted without precise knowledge of the dynamics. Since we can only predict the resting values of $\mathbf{r}_3$ and t_z, we will only consider the three-dimensional "slice" of the *C-space* given by $\mathbb{R} \times S^2$ when defining capture regions.

As in (Kriegman 1992), a configuration is considered stable if it is a local minimum of $u(\mathbf{q})$ over *C-free* $\cup$ *C-contact*. Since the potential energy decreases monotonically with translation along $\mathbf{g}$, the minimum of $u(\mathbf{q})$ must occur when the hull contacts the support plane, i.e., $\mathbf{q} \in$ *C-contact*. For a fixed orientation, contact occurs at a unique height, and so t_z and consequently u can be written as functions of $\mathbf{r}_3$. Taken together, one rotational and all translational degrees of freedom can be ignored. Thus, the relevant configuration space is equivalent (diffeomorphic) to a sphere, and we can define the potential energy function, which will still be denoted $u(\mathbf{q})$, as a map from the sphere $u\colon S^2 \to \mathbb{R}$; S^2 will then be partitioned into a set of capture regions.

4 Smooth Hulls and Morse Theory

In Section 2, the relationship between the dynamics of dissipative mechanical systems and potential functions was explored. In particular, for a bounded, closed, connected subset $\mathcal{S}$ of the configuration space, if $u(\mathbf{q}) = u_b$ is constant on the boundary of $\mathcal{S}$ and if $u(\mathbf{q}) < u_b$ on the interior, then $\mathcal{S}$ is an invariant set. Furthermore, we noted that if $u(\mathbf{q})$ is *uniminimal* (possessing only one minimum) on $\mathcal{S}$, then for any initial configuration $\mathbf{q}(t_0) \in \mathcal{S}, \dot{\mathbf{q}}(t_0) = 0$, the pose will converge to the local minimum for any totally dissipative system.[2] These are the conditions for $\mathcal{S}$ to be a capture region. So the question is, "For each minimum, how do we compute the largest (maximal) capture region, its boundary, and the value of u_b?" To answer this, we turn to Morse theory (Milnor 1963).

Following (Goresky & Macpherson 1980), let X be a compact differentiable manifold and f be a smooth, real valued function $f : X \to \mathbb{R}$. For a given real number r, consider the subset of X defined by $X_{\leq r} \equiv \{\mathbf{x} \in X : f(\mathbf{x}) \leq r\}$. Morse theory considers the topological changes to the set $X_{\leq r}$ as r varies. Note that $X_{\leq r}$ is a manifold (with boundary), and it may be composed of a set of disjoint, multiply connected components. Now, recall that a point $\mathbf{x} \in X$ where the differential df of f vanishes is called a *critical point* of f, and the corresponding value of $f(\mathbf{x})$ is called a *critical value*.

Theorem 1 *Let f be a differentiable function on a compact smooth manifold X. As r varies within the open interval between two adjacent critical values, the topological type of $X_{\leq r}$ remains constant. (Goresky & Macpherson 1980)*

For computing capture regions, X is diffeomorphic to S^2 as discussed in Section 3, and the function f is simply the potential energy function $u(\mathbf{q})$ defined on the sphere. Along the boundary of $S^2_{\leq u}$, the value of $u(\mathbf{q})$ is a constant u. If a connected component of $S^2_{\leq u}$ contains only one minimum, it defines a capture region. Since $X_{\leq r} \subseteq X_{\leq r'}$ for $r < r'$ from the definition, it may be possible to expand a capture region by increasing u. However as u is increased, a connected component may fail to remain a capture region if a second minimum is introduced to the region. It will be shown below that a new minimum can only be introduced to $S^2_{\leq u}$ by introducing a new disjoint set homeomorphic to a disk that contains the minimum. Thus, two connected components of $S^2_{\leq u}$ must merge for a second minimum to be added to an existing capture region. By Theorem 1, this topological change to $S^2_{\leq u}$ only occurs at critical points. Consequently, for a capture region to be maximal, the potential energy along the boundary must be a critical value of $u(\mathbf{q})$. If not, a capture region could be expanded without introducing a second minimum.

We will assume that $u(\mathbf{q})$ is a Morse function (Guillemin & Pollack 1974) (i.e. that the Hessian matrix of second derivatives of $u(\mathbf{q})$ is nonsingular at all critical points).[3]   During the process

---

[2]This is not strictly true when the configuration space is 2-D or greater. For example, if $\mathcal{S}$ is 2-D and punctured, and if the boundary of $\mathcal{S}$ is composed of n curves, then $\mathcal{S}$ contains $n - 1$ saddles of $u(\mathbf{q})$ (Koditschek 1991; Rimon & Koditschek 1992). For each saddle $\mathbf{h}$, there is a codimension 1 invariant set $\mathcal{S}' \subset \mathcal{S}$; for an initial configuration $q \in \mathcal{S}'$, $\mathbf{q}(t)$ will remain in $\mathcal{S}'$ and converge to $\mathbf{h}$ rather than the minimum. Fortunately, since $\mathcal{S}'$ is a set of measure zero, the initial configuration is unlikely (probability zero) to be on $\mathcal{S}'$. Thus, the presence of saddle points within a capture region will not be of practical concern.

[3]Assuming that $u(\mathbf{q})$ is Morse is not very restrictive since nearly all functions are Morse (i.e. in the space of smooth functions, the set of functions with degenerate critical points is of codimension one) (Milnor 1963). Furthermore, even if $u(\mathbf{q})$ were not Morse, the ideas of (stratified) Morse Theory can be extended to consider "nondepraved critical points." See (Goresky & Macpherson 1980).
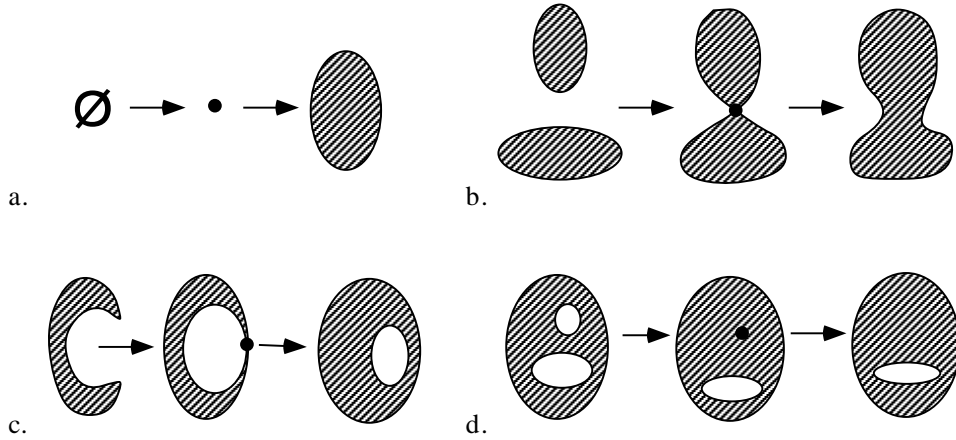
Figure 2: Changes to a capture region (a subset of $S^2_{\leq u}$) in the neighborhood of a critical point as u is increased and crosses a critical value: a. local minimum; b. type I saddle; c. type II saddle; d. local maximum.

of computing capture regions, it is easy to determine if $u(\mathbf{q})$ is Morse by computing the Hessian matrix at each critical point and checking that its determinant is nonzero. A sphere whose center of gravity is at the geometric center provides an example of an object whose potential energy function is not Morse; in this case, $u(\mathbf{q})$ is constant. However, any perturbation of $\mathbf{c}$ will make $u(\mathbf{q})$ Morse. Thus, only objects with Morse potential energy functions will be considered since perturbing $\mathbf{c}$ by simply adding a small random number to the coordinates of $\mathbf{c}$ will make $u(\mathbf{q})$ Morse.

Theorem 1 tells us that the topology of $X_{\leq r}$ only changes at critical points. Furthermore, the *Morse index* at a critical point (defined to be the number of negative eigenvalues of the Hessian matrix) can be used to determine how the topology of $X_{\leq r}$ changes when r crosses a critical value. Here, the Morse index can take on a value of 0, 1 or 2 since the Hessian matrix of $u(\mathbf{q})$ is 2×2. The change in topology is represented by the *Morse Data* which is a pair of spaces (A, B) with $B \subset A$. The change to $X_{\leq r}$ as r crosses a critical value can be described by "gluing in" A along B.

Theorem 2 *Let f be a Morse function on an n-dimensional smooth manifold X. Morse data measuring the topological change in $X_{\leq r}$ as r crosses the critical value of a critical point p is given by the "handle" $(D^\lambda \times D^{n-\lambda}, \partial D^\lambda \times D^{n-\lambda})$ where λ is the Morse index of f at p, D^i denotes a closed i-dimensional disk, and ∂D^i denotes its boundary (an $i - 1$ dimensional sphere). (Goresky & Macpherson 1980).*

In our case, when the $\lambda = 0$, the critical point $\mathbf{q}_c$ is a local minimum of $u(\mathbf{q})$, and the Morse data is $(D^2, \emptyset)$; the change in the topology of $S^2_{\leq u}$ as u crosses the critical value is to introduce a set homeomorphic to a disk to $S^2_{\leq u}$. When $\lambda = 1$, $\mathbf{q}_c$ is a saddle point, and the topological change is equivalent to gluing opposite sides of a rectangle to two disjoint boundary segments of $S^2_{\leq u}$. Finally when $\lambda = 2$, $\mathbf{q}_c$ is a local maximum, and the topological change is equivalent to gluing a disk along its boundary to $S^2_{\leq u}$. Figure 2 illustrates these changes.

Now, let us consider the level sets of the potential energy function. By the Implicit Function Theorem, the set of equipotential points on S^2 for some constant u_b (i.e. $\{\mathbf{q} \in S^2 : u(\mathbf{q}) = u_b\}$) form curves (*equipotential contours*) which are smooth except at isolated critical points. Furthermore
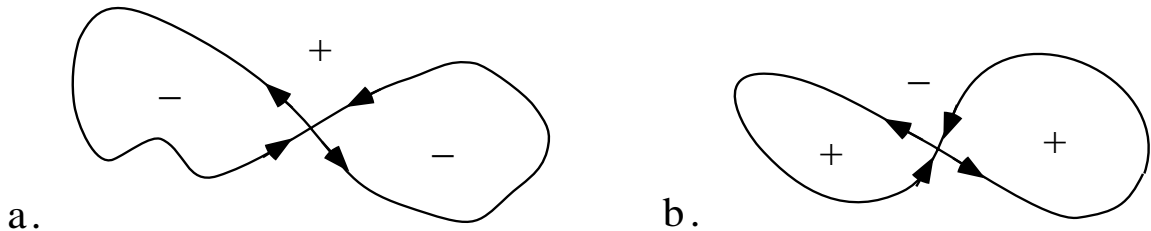
Figure 3: There are two qualitatively different ways that an equipotential contour through a saddle can divide the sphere S^2 into three regions. The signs indicate the relative potential energy with respect to the equipotential contour, and the arrows indicate the directions of departure and approach when tracing an equipotential contour.

because S^2 is bounded, the graph of potential energy is also bounded. Consequently, so are the equipotential contours. In general, they form simple closed loops. However, there is a transverse crossing at a saddle point, and when the critical values are distinct, the equipotential contour forms a figure-eight with two closed loops.

As shown in Figure 3, the equipotential contour through the saddle point divides the sphere into three disjoint regions. In the neighborhood of the contour, there are two qualitatively different cases. As in Figure 3.a, the potential energy immediately within the two loops is lower than on the equipotential contour; it is greater outside of the loops. The saddle essentially separates the two "valleys." In contrast, the potential energy is greater within the two loops in Figure 3.b. In this case, the saddle separates the two peaks. Note that the two cases cannot be distinguished from the geometry of $u(\mathbf{q})$ in the neighborhood of the saddle. However, if the two equipotential loops are traced, the directions of departure and of approach to the saddle can be determined for each loop. These directions are the asymptotic directions of the graph of $u(\mathbf{q})$. Now consider the principal direction (do Carmo 1976) lying between the approach and departure directions. If the principal curvature in this direction is negative (respectively positive), the saddle is qualitatively similar to that shown in Figure 3.a (respectively Figure 3.b).

The implications for computing capture regions of Theorem 2 follow: Every connected component of $S^2{}_{\leq u}$ must contain a local minimum of $u(\mathbf{q})$ since new components are introduced at critical points with $\lambda = 0$ (See Figure 2.a). We now consider what happens to a uniminimal connected component of $S^2{}_{\leq u}$ as u is increased and a critical value is crossed. To visualize these cases, consider the graph of the potential energy function on the sphere which is like a hilly globe. The set $S^2{}_{\leq u}$ is the portion of the globe where the altitude of the graph is less than u. There are a few cases:

1. If the critical point is a saddle ($\lambda = 1$), a handle is "glued" in. There are two subcases:

   (a) The saddle point is like that shown in Figure 3.a, and the handle joins two disjoint connected components of $S^2{}_{\leq u}$. Each component possesses at least one local minimum, and so after joining, $u(\mathbf{q})$ will no longer be uniminimal on the resulting component. Thus, the boundary of the maximal capture region is one of the equipotential contours through the saddle point. We term this a *type I saddle* (See Figure 2.b).

   (b) The saddle point is similar to the one in Figure 3.b, and the handle joins two parts of the boundary of the same uniminimal connected component. Since the sphere is orientable,

the resulting region is homeomorphic to a punctured disk. Note that this implies that a capture region may not be simply connected. We call this a *type II saddle* (See Figure 2.c). Subsequent type II saddles introduce additional punctures.

2. If u passes a critical value corresponding to a local maxima ($\lambda = 2$), a disk is "glued" in along its boundary, and there are two possibilities:

(a) If $S^2_{\leq u}$ is a disk, the result of the gluing operation is S^2; there is only one stable pose.

(b) Alternatively, the uniminimal component may be punctured, and the gluing operation will eliminate a puncture (See Figure 2.d).

This completely enumerates the possible changes to the topology of a uniminimal connected component of $S^2_{\leq u}$ as u increases and crosses a critical value. From this catalogue, we can conclude that a type I saddle point determines the potential energy u_b along the boundary of a maximal capture region (except in the trivial case where the region is all of S^2).

We also note that a uniminimal capture region may contain critical points (maxima and saddles) besides the single minimum; however, these critical points are not stable. For an initial configuration along a particular collection of curves in the region called the *stable manifold* of a saddle point, the dynamical system will converge to one of the saddle points. However, the stable manifold is a set of measure zero, and these other critical points are unstable, so including these critical points within the capture region should not cause any trouble in practice. For each capture region, there are at least two critical points (the minimum and a saddle on the boundary). A capture region will contain more than two critical points only when the second critical point (ordered by increasing critical value) is a type II saddle, and the capture region is equivalent to a punctured disk.

A useful fact to note is that because $u \colon S^2 \to \mathbb{R}$ is a mapping from a surface of genus zero whose Euler characteristic χ is two, a consequence of the Poincaré-Hopf Theorem (Guillemin & Pollack 1974) is: $N_{min} + N_{max} - N_{sad} = \chi$ where N_{min}, N_{max} and N_{sad} are respectively the number of minima, maxima and saddles. In practice, this serves as a check when computing and characterizing the critical points of $u(\mathbf{q})$ for a particular object.

4.1 Algorithm for Determining Capture Regions

The above discussion suggests the following algorithm for computing the maximal capture regions of an object with a smooth convex hull $\mathcal{H}$ given the location of its center of gravity $\mathbf{c}$. Details will be provided subsequently.

4.1.1 An Outline of the Algorithm

A uniminimal region of S^2 is represented by a minimum $\mathbf{q}_m$ and a discrete approximation to the set of closed equipotential contours bounding the region; the potential energy is constant u_b on these contours. The output of the algorithm is a list of maximal capture regions.

1. Set the `region-list` to empty;

2. Compute all critical points $\mathbf{q}_c$ using global methods and determine their Morse indices;

3. Sort the critical points by increasing critical value $u_c = u(\mathbf{q}_c)$;

9

4. Looping through the critical points, if $\mathbf{q}_c$ is a:

Minimum: Create a new region with $\mathbf{q}_m = \mathbf{q}_c$ and $u_b = u_c$, and add it to the `region-list`.

Saddle: Trace the two closed equipotential contours $\mathcal{L}_1, \mathcal{L}_2$ through $\mathbf{q}_c$. For each $\mathcal{L}_i$, integrate a dissipative system starting from some $\mathbf{q}(0) \in \mathcal{L}_i$ until $\mathbf{q}(t)$ converges upon a minimum $\mathbf{q}_{m_i}$. The type of the saddle is determined as follows:

When $\mathbf{q}_{m_1} \neq \mathbf{q}_{m_2}$, $\mathbf{q}_c$ is a **type I saddle**. For each $\mathbf{q}_{m_i}$, if it lies within a region on the `region-list`, then $\mathcal{L}_i$ encloses $\mathbf{q}_{m_i}$, and $\mathcal{L}_i$ forms a boundary of the maximal capture region of $\mathbf{q}_{m_i}$. If this region is punctured, $\mathcal{L}_i$ replaces an existing boundary, and the other boundaries are smoothly deformed by increasing the energy from u_b to u_c. This completely defines a maximal capture region; delete it from the `region-list`.

When $\mathbf{q}_{m_1} = \mathbf{q}_{m_2}$, $\mathbf{q}_c$ is a **type II saddle**. $\mathcal{L}_1$ and $\mathcal{L}_2$ both become boundaries of the region (introducing a puncture). One of these replaces an existing boundary while the other is new. Smoothly deform any other contours by increasing the energy from u_b to u_c.

Maximum: Determine if a punctured uniminimal region surrounds the maximum. Eliminate the corresponding contour, and smoothly deform the remaining contours by increasing the energy from u_b to u_c.

4.1.2 Specifics for Implicit Surfaces

Many of the steps described above are involved; we now provide details for the case when $\mathcal{H}$ is defined implicitly. Except for one step, determining the critical points, the approach is general. In that one step, the surface must be algebraic. Consider $\mathcal{H}$ to be represented as the zero set of a $\mathcal{C}^3$ function:

$$f(\mathbf{p}) = 0 \qquad (2)$$

where $\mathbf{p} \in \mathbb{R}^3$. The Gauss map $n: \mathcal{H} \to S^2$, yielding the outward pointing unit surface normal, is

$$\mathbf{n}(\mathbf{p}) = \frac{1}{|\nabla f(\mathbf{p})|} \nabla f(\mathbf{p}) \qquad (3)$$

where ∇ denotes $\partial/\partial \mathbf{p}$.

Since $\mathcal{H}$ is convex and bounded, and $\mathbf{n}(\mathbf{p})$ is defined everywhere on $\mathcal{H}$, the Gaussian image of $\mathcal{H}$ covers the sphere S^2. Thus, the Gauss map is surjective. For convenience, we also assume that it is injective; this allows us to invert the Gauss map, $n^{-1}: S^2 \to \mathcal{H}$. Note that when $\mathcal{H}$ is a bounded convex algebraic surface, it can be shown that the Gauss map is necessarily injective. Furthermore, we can identify the surface normal with a configuration of the object in contact with the supporting plane. Thus, we arrive at the following pair of maps.

$$S^2 \xleftarrow{\mathbf{n}} \mathcal{H} \xrightarrow{u} \mathbb{R}$$

Since the Gauss map is assumed to be invertible, all of the necessary calculations can be calculated on $\mathcal{H}$ rather than on S^2. This is much more convenient because while the Gauss map is explicitly given by (3), there is no explicit expression for its inverse. The algorithm outlined above can be recast in terms of points on the surface of the hull rather than over points in the configuration space. The equations in the rest of this section will be expressed in terms of the coordinates of the

point of contact $\mathbf{p}$ on $\mathcal{H}$; the coordinates of $\mathbf{c}$ are then constant. As a map $u: \mathcal{H} \to \mathbb{R}$, the potential energy is given by:

$$u(\mathbf{p}) = (\mathbf{p} - \mathbf{c}) \cdot \mathbf{n}(\mathbf{p}) \tag{4}$$

4.1.3   Computing Critical Points

The critical points of (4) are given by $du = 0$; differentiating (4) and (2) and eliminating $d\mathbf{p}$, we obtain:

$$(\mathbf{p} - \mathbf{c}) \times \mathbf{n}(\mathbf{p}) = \mathbf{0} \tag{5}$$

which is a system with two linearly independent equations. Equation 5 simply states that $\mathbf{p} - \mathbf{c}$ is aligned with the surface normal at the critical points (Kriegman 1992). Along with $f(\mathbf{p}) = 0$, this yields a system of three equations in three unknowns which can be solved for $\mathbf{p}$.

As shown in (Kriegman 1992), the classification of a critical point can be determined from the principal curvatures k_1, k_2 of the surface at $\mathbf{p}$. Let us assign principal directions so $k_1 \leq k_2$. Because $\mathcal{H}$ is convex, the contact point must be either elliptic or parabolic, and so k_1 and k_2 must be non-negative. Define $k_c = 1/|\mathbf{p} - \mathbf{c}|$ to be the curvature of a sphere centered at $\mathbf{c}$ and making second order contact with $\mathcal{H}$ at $\mathbf{p}$ (i.e., the tangent planes of the sphere and $\mathcal{H}$ are identical at $\mathbf{p}$). If $k_c < k_1$, the critical point is a local maximum of $u(\mathbf{p})$. If $k_1 < k_c < k_2$, the point is a saddle, and if $k_c > k_2$, then the point is a local minimum. Note that when $k_c = k_1$ or $k_c = k_2$, $u(\mathbf{q})$ is not a Morse function; for a smooth hull, these are the only conditions where $u(\mathbf{q})$ is not Morse.

To actually compute the principal curvatures for a surface defined implicitly, we follow (do Carmo 1976) and note that the differential of the Gauss Map evaluated at a point $\mathbf{p}$ $dn: T_p \to T_p$ is given by $dn(\mathbf{v}) = DN\mathbf{v}$ where DN is a 3×3 matrix evaluated at $\mathbf{p}$ with elements $DN_{ij} = \partial\mathbf{n}_i/\partial\mathbf{p}_j$; i, j denote coordinates of $\mathbf{n}$ and $\mathbf{p}$. For a surface given implicitly, DN is expressed as:

$$DN = \frac{1}{|\nabla f|}(I - \mathbf{n}\mathbf{n}^t)H$$

where H is the Hessian matrix of $f(\mathbf{p})$. The normal curvature at $\mathbf{p}$ in the direction $\mathbf{v}$ is given by second fundamental form or $k_n(\mathbf{p}, \mathbf{v}) = -\mathbf{v}^t DN\mathbf{v}$. Note that DN is a rank two matrix. Two of the eigenvectors of DN lie in the tangent plane and are the principal directions of the surface; their corresponding eigenvalues are the principal curvatures k_1 and k_2.

4.1.4   Tracing Equipotential Contours

The algorithm outlined above requires tracing an equipotential contour from some initial point $\mathbf{p}_0$ on the contour whose potential energy is $u_b = u(\mathbf{p}_0)$. While a general algebraic curve tracing routine such as (Kriegman & Ponce 1991) could be employed, this is unnecessary since we have assumed that $u(\mathbf{q})$ is a Morse function. As noted in Section 4, the equipotential contours form closed curves whose only singularities occur at saddle points where a transverse crossing occurs. Starting at $\mathbf{p}_0$, a sequence of points on the curve is found using a traditional curve marching technique composed of prediction and correction steps.

Along the equipotential contour, $\dot{u}(\mathbf{p}) = 0$. So if $\mathbf{p}$ is a regular point of the contour, the tangent $\mathbf{t}$ to the equipotential contour can be determined by differentiating (2) and (4) and solving for $\mathbf{t} = \dot{\mathbf{p}}$. This yields

$$\mathbf{t} = \nabla f \times DN^t(\mathbf{p} - \mathbf{c}) \tag{6}$$

11

where DN^t denotes the transpose of DN. To predict the next point $\mathbf{p}_{i+1}$ along the equipotential contour from a point $\mathbf{p}_i$, a step of length δ is taken in the direction $\mathbf{t}$ by $\mathbf{p}_{i+1} = \mathbf{p}_i + (\delta/|\mathbf{t}|)\mathbf{t}$.

In general, the predicted point $\mathbf{p}_{i+1}$ will be near the equipotential contour, and an improved (corrected) estimate can be obtained by applying Newton's method in a direction orthogonal to $\mathbf{t}$; $\mathbf{p}_{i+1}$ is repeatedly corrected according to $\mathbf{p}_{i+1} \leftarrow \mathbf{p}_{i+1} + \mathbf{\Delta}$ where the correction $\mathbf{\Delta}$ is found by solving the following linear system:

$$
\begin{bmatrix} \mathbf{p}^t_{i+1} \\ (\mathbf{p}_{i+1} - \mathbf{c})^t DN \\ \nabla f^t(\mathbf{p}_{i+1}) \end{bmatrix} \mathbf{\Delta} = - \begin{bmatrix} 0 \\ u(\mathbf{p}_{i+1}) - u_b \\ f(\mathbf{p}_{i+1}) \end{bmatrix}
\tag{7}
$$

For nearly all points on the contour, this tracing procedure works well in practice. The only difficulty arises when $\mathbf{p}_i$ is a saddle point and (6) vanishes. At these points, the equipotential contour is singular and forms a regular crossing. The tangent directions of the two branches at the crossing are given by the asymptotic directions of the graph of the potential energy function. This can be expressed as the solution to the following two homogeneous equations in $\mathbf{t} = (t_x, t_y, t_z)$.

$$
\begin{cases} \nabla f(\mathbf{p}) \cdot \mathbf{t} = 0 \\ (\mathbf{p} - \mathbf{c})^t [t_x DN_x + t_y DN_y + t_z DN_z]\mathbf{t} + \mathbf{t}^t DN\mathbf{t} = 0 \end{cases}
$$

where DN_x denotes the matrix of partial derivatives of DN with respect to x evaluated at $\mathbf{p}$.

4.1.5 Associating Minima

To determine if a minimum $\mathbf{p}_{m_i}$ is enclosed by an equipotential contour $\mathcal{L}_i$ passing through a saddle point in Step 4 of the algorithm, a differential equation describing some dissipative system can be integrated starting at zero velocity $\dot{\mathbf{p}}(t_0) = 0$. Since $u(\mathbf{p})$ is singular at a saddle point, a point on each traced loop is used as the initial configuration $\mathbf{p}(t_0)$. Now what form should the differential equations take? If $\mathcal{L}_i$ delimits a uniminimal region, then *any* dissipative system will converge to the minimum of that region. For simplicity, we choose the gradient of the potential energy function

$$
\dot{\mathbf{p}}(t) = \nabla u(\mathbf{p}(t))
\tag{8}
$$

restricted to the tangent plane of $\mathcal{H}$ at $\mathbf{p}(t)$. While this system will not converge within finite time, it is integrated until the distance of $\mathbf{p}(t)$ to some minimum is less than some ϵ. Recall that the set of minima have been computed already, so it is easy to determine when to terminate. If the minimum lies within a region on the `region-list`, $\mathcal{L}_i$ becomes a new boundary of that region. If the system converges to the same minimum on `region-list` for both initial points, the saddle point must be a type II saddle, and both $\mathcal{L}_1$ and $\mathcal{L}_2$ become bounding contours of the capture region.

To determine if a maximum $\mathbf{p}$ closes a puncture of a uniminimal region, $\mathbf{p}$ is perturbed from the maximum in any direction, and the gradient system (8) is integrated starting from the perturbed $\mathbf{p}$. If the system converges to within ϵ of a minimum on the `region-list`, the maximum closes a puncture of that region. Since $u(\mathbf{p}(t))$ decreases monotonically, the trajectory $\mathbf{p}(t)$ can only cross one of the boundary contours of the uniminimal region; this contour can be eliminated from the uniminimal region.
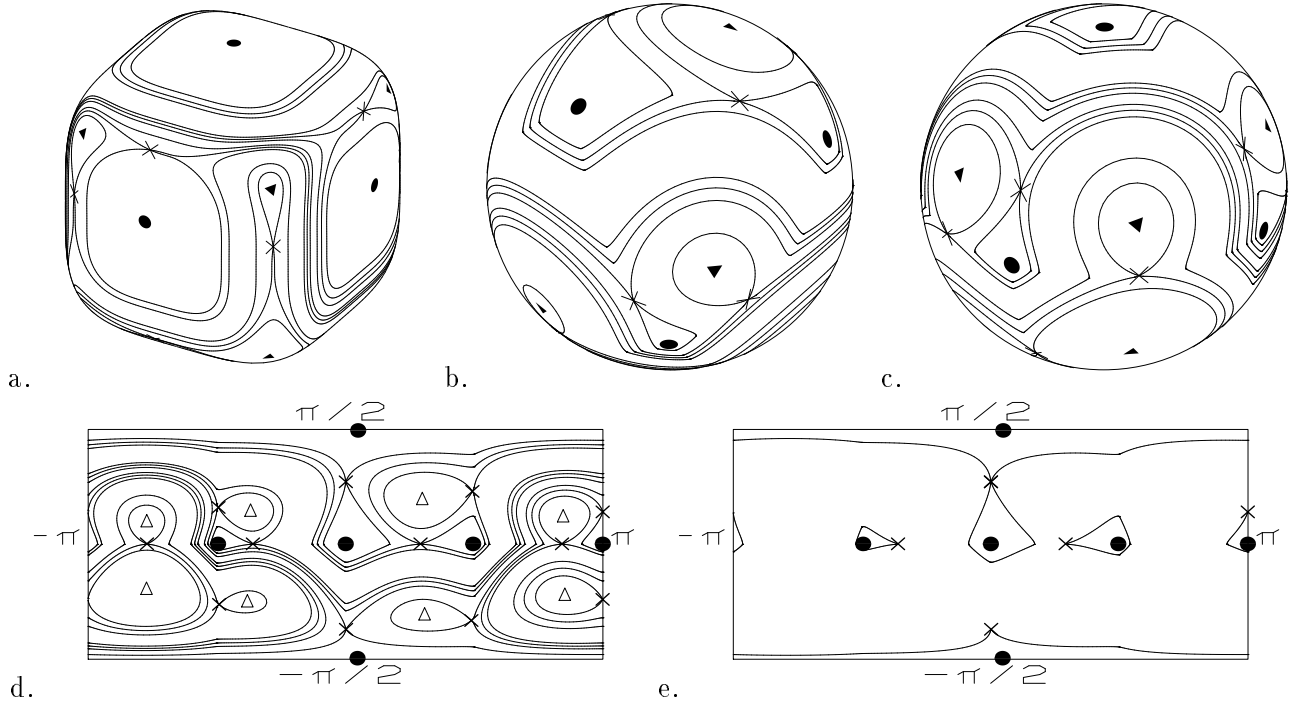
Figure 4: Capture regions of a superellipsoid whose center of gravity is off-center: The critical points and equipotential contours are drawn on the surface in (a), are seen in two views of the sphere in (b and c), and are drawn spherical coordinates in (d). The triangles, circles and x's respectively indicate maxima, minima and saddles; e. The capture regions are drawn in spherical coordinates.

4.1.6 Pushing up equipotential contours

When a uniminimal region on the `region-list` is punctured, a subsequent saddle or maximum leads to a change in the region's connectivity. The new boundary curves are determined by the equipotential contours at energy u_c through the critical point. While the potential energy of the contours were u_b, these boundaries need to be "lifted" to have potential, u_c. Since Theorem 1 states that the connectivity of a region and hence the boundaries only changes at a critical point, the boundaries that do not pass through the critical point can be smoothly deformed. Rather than continuously deforming the contour, a single point $\mathbf{p}_0$ on each contour is "deformed" by integrating the negative gradient system $\dot{\mathbf{p}}(t) = -\nabla u(\mathbf{p}(t))$ restricted to the tangent plane at $\mathbf{p}(t)$ from $\mathbf{p}_0$ until $u(\mathbf{p}(t_f)) = u_c$. After integration, the equipotential contour can be traced using the algorithm of Section 4.1.4 starting at $\mathbf{p}(t_f)$.

4.2 Implementation and Examples

The algorithm for computing the maximal capture regions described in Section 4.1 has been implemented for a convex hull $\mathcal{H}$ represented by an algebraic surface. Below, examples of applying the algorithm to two objects (superellipsoids) are presented. In both cases, the center of gravity $\mathbf{c}$
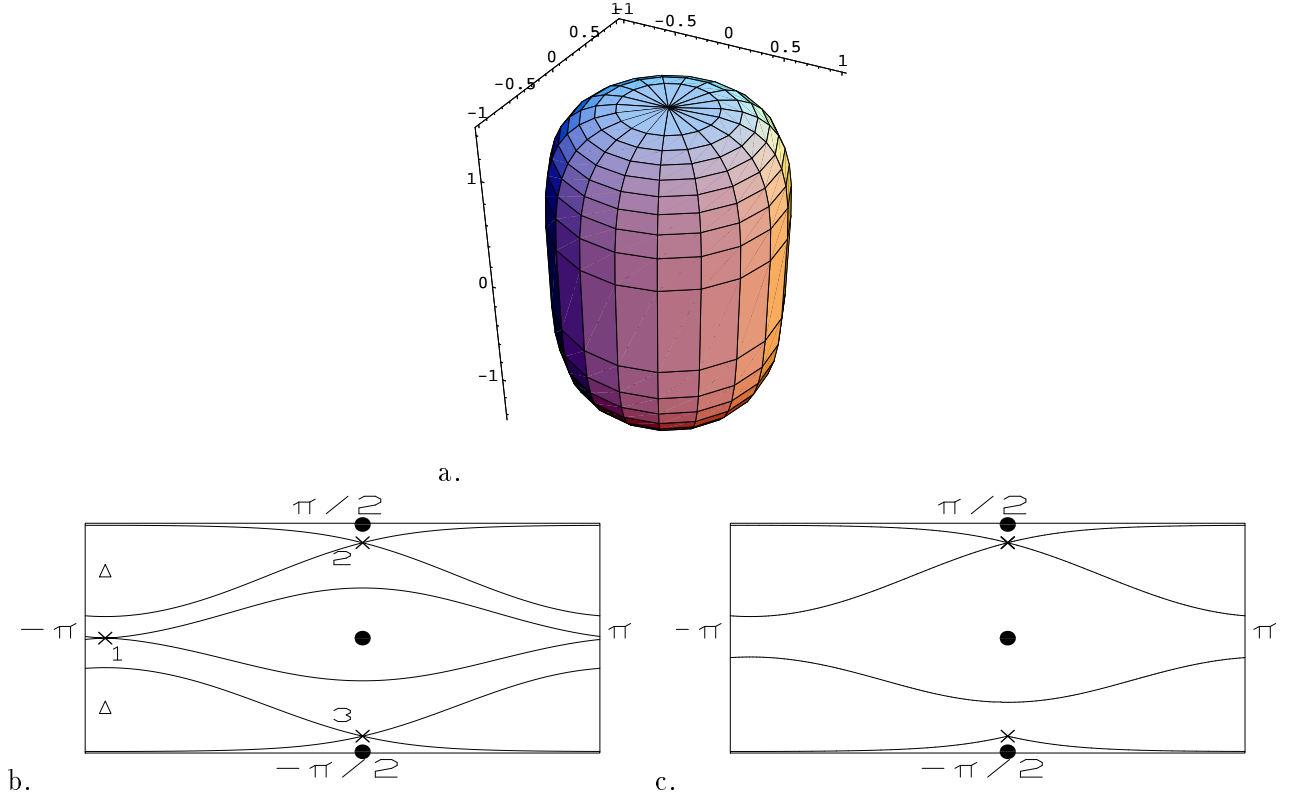
a.

b.

c.

Figure 5: Capture regions of another superellipsoid: a. the superellipse; b. critical points and equipotential contours; c. the capture regions. Note that the central region is homeomorphic to an annulus.

does not lie at the geometric center of the object; this ensures that $u(\mathbf{q})$ is a Morse function. By applying the algorithm to algebraic surfaces, the global method of homotopy continuation can be used to determine the coordinates of the critical points (Morgan 1987). This is the only part of the algorithm that requires $\mathcal{H}$ to be an algebraic surface. In the presented examples, a distributed implementation of homotopy continuation running on a network of four workstations is used to solve these systems; the polynomial systems have a total degree ranging up to 64 and are solved in less than thirty seconds. The rest of the implementation is written in Common Lisp, and the two examples presented below ran on a Sun SPARC Station I in a total 8.5 minutes and 4.5 minutes.

The first example shown in Figure 4.a is a superellipsoid whose equation is $x^4 + y^4 + z^4 - 16 = 0$ and whose center of gravity is $\mathbf{c} = (.45, .25, .35)$. There are 26 critical points (6 minima, 12 saddles, and 8 maxima). This agrees with the Euler characteristic. Figure 4.a shows the critical points along with the equipotential contours drawn on the surface. Each capture region corresponds to a portion of the surface containing a minimum (a circle) and the innermost equipotential contour. For an initial point of contact within this region, the part will settle to the corresponding stable pose. Note that in practice, it is unnecessary to trace all of these contours when computing the capture regions; while looping through the critical points, if the `region-list` is empty, the equipotential contours emanating from a saddle point cannot delineate a uniminimal region. From antipodal

14

viewpoints, Figures 4.b and 4.c portray the critical points and equipotential contours on the sphere while Figure 4.d shows them in spherical coordinates. Be aware that this grossly distorts the geometry in the neighborhood of the two poles (top and bottom) and that the left and right sides of the figure are identified — so, the contours wrap around this boundary. Finally, Figure 4.e shows the capture regions; each one is homeomorphic to a disk.

As discussed in Section 4 and illustrated in Figure 5, a capture region may contain punctures. The superellipsoid defined by $(x^2 + y^2)^2 + (z/1.4)^4 = 1$ with center $\mathbf{c} = (.2, .05, .05)$ has a circular cross section in the x-y plane and a superelliptic cross section in the x-z plane. It is easy to visualize the three stables poses: two of them involve contact on the flat ends; since $\mathbf{c}$ is off-center, there is also another stable pose where the point of contact lies on the "cylindrical" portion of the surface. As shown along with the equipotential contours in Figure 5.b, there are only 8 critical points (three minima, three saddles and two maxima). The numbers in Figure 5.b indicate the increasing potential of the three saddles. Saddle 1 is a type II saddle; the two smooth contours surround the central minimum. Saddle 2 is a type I saddle, and the two equipotential contours individually surround the central and upper minima. As shown by the capture regions in Figure 5.c, the contour through Saddle 2 replaces the upper contour through Saddle 1. The lower contour in Figure 5.b through Saddle 1 is pushed up to the same potential as Saddle 2 using the method of Section 4.1.6 and does not pass through a critical point as seen in Figure 5.c. Thus, the capture region of the central minimum is a band that wraps around the equator.

5   Piecewise-smooth Objects

Until this point, we have restricted our attention to objects whose convex hulls are at least thrice differentiable; this allowed us to apply Morse theory to study the changes in topology of the configuration space under the potential energy function. Here we turn toward more realistic models of objects, and allow a part to have a convex hull $\mathcal{H}$ composed of smooth surface patches that join along intersection curves which meet at vertices. This includes the important subclass of polyhedra.

The discussion will follow the one presented for smooth hulls. We will consider the potential energy function defined on the object's configuration space and construct maximal uniminimal regions of the *C-space*. Again, we will consider the changes to the connectivity of the regions as potential energy increases. We will be particularly interested in those events that create new uniminimal regions, that join two regions together, and that close punctures.

There are a few points to note about this extended class of objects. First, since the convex hull is not smooth, the potential energy function is not smooth, and so Morse theory cannot be directly applied. Fortunately, recent extensions called stratified Morse theory can be used to generate a catalogue of generic topological changes. The second point to note concerns the use of the Gauss map between $\mathcal{H}$ and S^2. When presenting the algorithm for algebraic surfaces in Section 4.1.2, we assumed that the Gauss map was injective, and so it could be defined in terms of points on $\mathcal{H}$ rather than on S^2. Here, we no longer have that luxury. Consider a polyhedron. A face resting on the supporting plane (a single configuration) has many points of contact. Alternatively, when a vertex (a single point) remains in contact with the plane, the object's configuration has two degrees of freedom. So, we will be forced to consider the map $u: S^2 \to \mathbb{R}$ directly.

In this section, we first present some definitions and results from stratified Morse theory and then apply these to computing capture regions. Unfortunately we will run into a problem imme-

diately. The author is not aware of a complete classification of the points on the convex hull of a general piecewise-smooth object. However, such catalogues exist for polyhedra, generic smooth surfaces (with concavities), and generic space curves. In this paper, only the first two cases will be considered. The development can be extended to the most general case – presently, the missing link is a complete catalogue of points on the convex hull.

5.1 Stratified Morse Theory

Whereas Morse theory is concerned with the change in topology of the set $X_{\leq r}$ for a differentiable function $f \colon X \to \mathbb{R}$ where X is a compact smooth manifold, stratified Morse theory (Goresky & Macpherson 1980) can be applied when X is a singular set, in particular a Whitney stratified set.

Any closed subset X of some d-dimensional manifold $X \subset M$ (e.g. $M = \mathbb{R}^d$) which can be decomposed into the finite union of disjoint manifolds (*strata*) of dimension ranging from 0 to d is called a *stratified set*. For example, a polyhedron can be decomposed into the union of its interior (a 3-manifold), its faces (2-manifolds), its edges (1-manifolds), and its vertices (points which are 0-manifolds). If it satisfies the Whitney conditions, then it is called a Whitney stratified set. We leave these conditions unstated because as noted in (Canny 1988), all semi-algebraic sets can be stratified in a manner which satisfies the Whitney conditions (Whitney 1957); algorithms such as cylindrical algebraic decomposition (Collins 1975) or Canny's roadmap are available for decomposing a semialgebraic set into strata. The importance of semialgebraic sets is that nearly all object models created by CAD systems are semialgebraic since they are composed of Boolean combinations of solids bounded by algebraic surfaces (e.g. planes, quadric surfaces, B-splines, NURBS, etc.). Note that the convex hull of a semialgebraic set is also semialgebraic. This can be seen by noting that the convex hull can be considered a *C-space* obstacle for the object interacting with a plane, and configuration space obstacles of semialgebraic sets are themselves semialgebraic (Latombe 1991).

Consider the restriction to a Whitney stratified set X of a smooth real valued function on M, $f \colon M \to \mathbb{R}$. A point $x \in X$ is considered a *critical point* of f if it is a critical point of the restriction of f to any stratum. Note that all zero dimensional strata are critical points. The corresponding *critical value* is then given by $v = f(x)$. Analogous to Theorem 1, we have

Theorem 3 *As r varies within the open interval between two adjacent critical values, the topological type of $X_{\leq r}$ remains constant (Goresky & Macpherson 1980).*

As with Theorem 1, the primary implication of this theorem is that we only need to consider the critical points to determine the capture regions. This theorem has recently been applied in Rimon and Canny's incremental motion planning algorithm (Rimon & Canny 1994).

Analogous to Theorem 2, the change in the topology of $X_{\leq r}$ as r crosses a critical value can be determined by applying the following theorem (the terms will be defined below):

Theorem 4 *Let f be a Morse function on a compact Whitney stratified space X. Then, Morse data measuring the change in the topological type of $X_{\leq r}$ as r crosses the critical value of a critical point p is the product of the normal Morse data at p and the tangential Morse data at p (Goresky & Macpherson 1980).*

The *tangential Morse data* at p is defined to be the Morse data for the restriction of f to the stratum S of X containing p, and from Theorem 2, it is equivalent to $(D^\lambda \times D^{n-\lambda}, \partial D^\lambda \times D^{n-\lambda})$
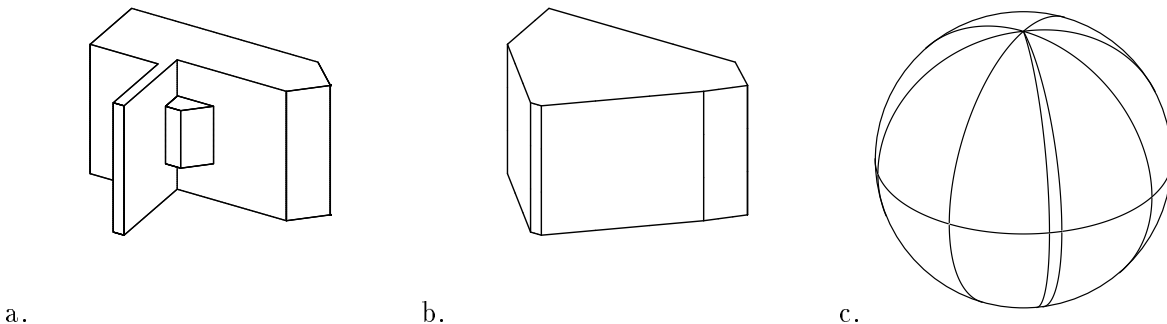
Figure 6: a. A polyhedron; b. its convex hull; c. the stratification of the spherical configuration space. Under the generalized normal, faces of the hull map to vertices, edges map to arcs of great circles, and vertices map to regions of the sphere.

where n is the dimension of S and λ is the Morse index. To define the normal Morse data at p, let N' be a smooth submanifold of M which is transverse to S at p such that $dim(S) + dim(N') = dim(M)$. The *normal slice* is then given by: $N(p) = N' \cap X \cap \mathcal{B}(p)$ where $\mathcal{B}(p)$ is a small ball in M around p. The *normal Morse data* at a critical point p with critical value $v = f(p)$ is then defined to be the pair of spaces (A, B) where $A = \{x \in N(p) : v - \epsilon \leq f(x) < v + \epsilon\}$ and $B = \{x \in N(p) : f(x) = v - \epsilon\}$ for some small ϵ. Finally, the product of a pair of topological spaces is given by $(A, B) \times (A', B') = (A \times A', A \times B' \cup B \times A')$. In Sections 5.3 and 5.4, tangential and normal Morse data will be explicitly computed. Theorem 4 has recently been used to compute the stable configurations of a part that is supported by multiple non-coplanar contacts (Mason, Rimon & Burdick 1995). These configurations correspond to local minima of potential energy and have Morse data of the form $(A, \emptyset)$ where A is nonempty.

Theorems 3 and 4 apply to a function f on M which is said to be Morse if (1) the critical values of the restriction of f to X are distinct; (2) for each stratum S of X, the critical points of f restricted to S are nondegenerate (nonsingular Hessian matrix); (3) $\nabla f(p)$ is not orthogonal to any of the other strata meeting at p. As with the classical definition of Morse functions, most smooth functions on a Whitney stratified set are Morse.

5.2 Convex Hulls and Configuration Space Revisited

An object contacts the supporting plane on its convex hull, and so we only need to consider computing capture regions of convex objects. It is well known that the convex hull of an arbitrary polyhedron is a polyhedron, and numerous implemented algorithms are available for constructing the hull (Preparata & Shamos 1985). Figure 6.a shows a polyhedral part while Figure 6.b shows its hull.

As discussed in (Arnol'd 1984; Koenderink 1990; Zakalyukin 1978), a catalogue of the regular and singular points on the convex hull of a generic smooth surface has been developed. Figure 7 presents this catalogue, and the example shown in Figure 8 will be considered below. The hull is composed of three types of regular points: points on the actual surface (Fig. 7.a), points on a bitangent developable surface for which each ruling has second order contact with the surface
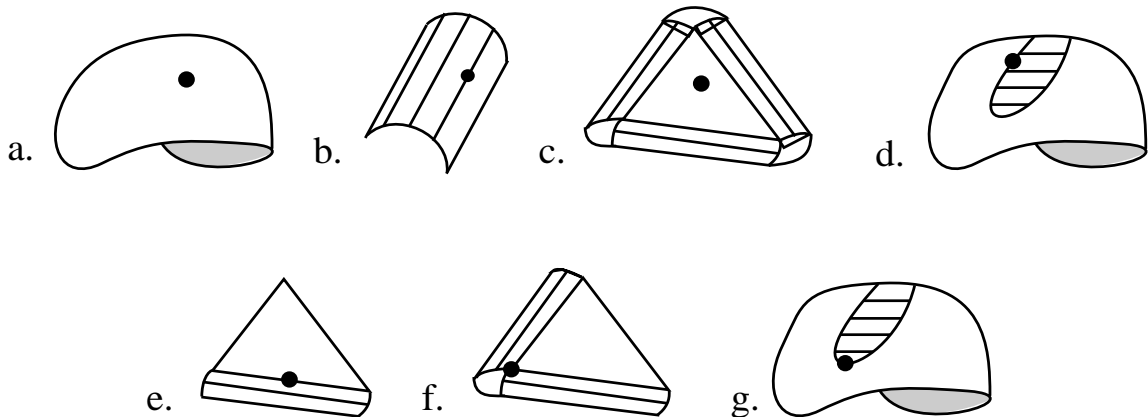
17

Figure 7: A catalogue of surface points on the convex hull of a generic smooth surface (adapted from (Koenderink 1990)).

at two points (Fig. 7.b), and points on a planar patch which makes second order contact with the surface at three points (Fig. 7.c). This catalogue of regular points holds for both the hull of smooth and piecewise-smooth objects. Patches of regular points meet along singular curves which join or terminate at singular points. For the convex hull of a smooth surface, there are two types of singular curves: points of contact between the bitangent developable surface and the part illustrated in Figure 7.d, and the line where the bitangent developable meets the tritangent plane shown in Figure 7.e. The singular points on the hull are either the vertices of a tritangent plane (Fig. 7.f) or an endpoint of a bitangent developable (Fig. 7.g). The later points, known as *godrons* (French for ruffle) (Koenderink 1990), are parabolic points which are cusps of the Gauss map (Banchoff, Gaffney & McCrory 1982); the direction of the bitangent developable is the sole asymptotic direction at the *godron*. The left side of Figure 8 shows a three humped object and its convex hull overlaid. In addition to points on the original surface, the hull includes one tritangent plane and three bitangent developable surfaces, each terminating at a *godron*.

Beyond smooth surfaces, (Sedykh 1977; Sedykh 1986) presented a catalogue of the normal forms of points on the convex hull of a generic space curve. There are two classes of regular points on the boundary of the hull: First, the regular point may lie on a developable surface where each developable contacts the space curve at two points. Second, a regular point may lie on a plane that contacts the curve at three points. The singular points of the hull include sections of the space curve as well as points where the two types of regular points meet. In fact, the developable generated by two edge curves may itself be singular (Arnol'd 1984).

Now consider a general piecewise-smooth part composed of vertices, edges (space curves), and regular surface points. The convex hull includes portions of the original part. Additionally, it includes planar patches and developable surfaces; the points of contact may be some combination of vertices, edge points or regular surface points. The various regular hull points meet at singular curves. Unfortunately, to the best of the author's knowledge, there is no complete catalogue of the singular points on the hull. Though Hung and Ierardi have recently presented a method for constructing the hull of piecewise-smooth objects, an explicit catalog of surface points does not emerge (Hung & Ierardi 1994). Subsequently, we will restrict our attention to polyhedra and
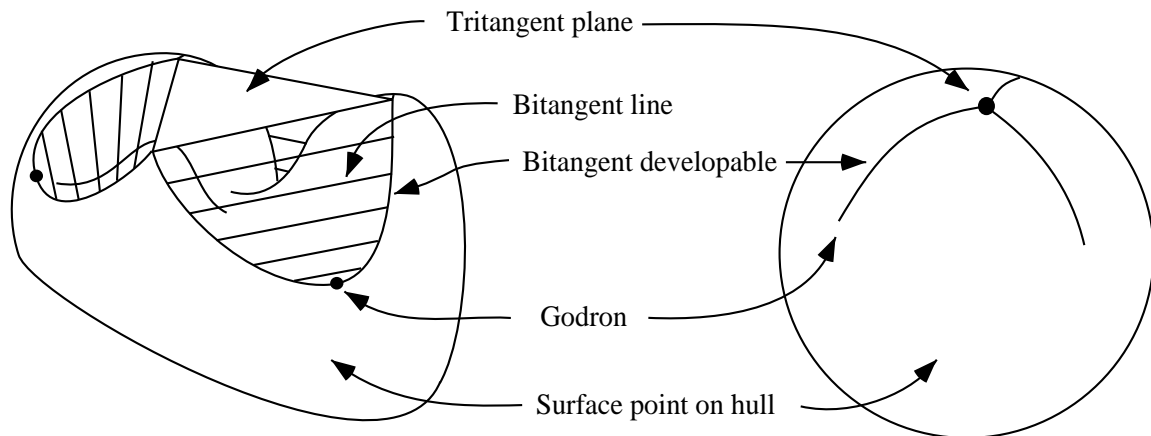
18

Figure 8: A smooth three-humped object with its convex hull and the corresponding stratification of the configuration space (adapted from (Koenderink 1990)).

smooth surfaces for which the catalogues are complete. The methodology described below can be readily applied to piecewise-smooth parts given a complete catalogue.

As in Section 4, the configuration space of a piecewise-smooth surface in contact with a support plane can be reduced to S^2, and the potential energy u can be defined on S^2. Since $\mathcal{H}$ is not smooth, the surface normal is not well defined at every point. However, from nonsmooth analysis (Clarke 1990), a generalization of the surface normal called the normal cone N_c at a point $\mathbf{x}$ can be employed and is defined as

$$N_c(\mathbf{x}) = co\{\mathbf{n} = \lim_{\mathbf{x}_i \to \mathbf{x}} \rho \mathbf{n}(\mathbf{x}_i) : \mathbf{x}_i \in F, \rho \in \mathbb{R}+\} \tag{9}$$

where $\mathbf{n}(\mathbf{x}_i)$ is the surface normal at $\mathbf{x}_i$, F is the set of two dimensional strata of $\mathcal{H}$ (the faces), co indicates the convex hull, and the limit is taken from all $\mathbf{x}_i \in F$. Note that in this definition, the normal $\mathbf{n}(\mathbf{x}_i)$ is only computed on the 2-D strata where it is well defined. The set of unit vectors within N_c, which will be termed the *generalized normal*, corresponds to the set of configurations for which the point $\mathbf{x}$ can contact the supporting plane. The generalized normal provides the relationship between the convex hull and the configuration space.

Under the generalized normal, a regular point on the hull maps to a single point on S^2 according to the Gauss map. In general a region of exposed regular points on $\mathcal{H}$ such as those in Fig 7.a maps to a region of S^2. Developable surfaces including planes are exceptional since all points along a single developable map to the same configuration on S^2. The intersection of two surfaces F_1 and F_2 defines a space curve $\mathbf{x}(s)$. The generalized normal at a single edge point is an arc on S^2 given by the convex combination of the surface normals $\mathbf{n}_1(s)$ and $\mathbf{n}_2(s)$ of F_1 and F_2 at $\mathbf{x}(s)$. When taken over the entire edge, the generalized normal sweeps a region of S^2 given by:

$$\mathbf{n}(s, \theta) = \cos \theta\, \mathbf{n}_1(s) + \sin \theta\, \mathbf{n}_2(s) \tag{10}$$

where θ ranges between 0 and $\pi/2$, and $\mathbf{n}(s, \theta)$ is unnormalized. In the special case when the edge is linear, $\mathbf{n}_1(s)$ and $\mathbf{n}_2(s)$ are constant vectors and $\mathbf{n}(s, \theta)$ collapses to a curve which can be written as $\mathbf{n}(\theta)$. From (9), the generalized normal at a vertex can be computed from the convex combination of the normals of all faces incident to the vertex. Thus, a vertex also maps to a region of S^2.

For the convex hull of the smooth surface shown in Figure 8, consider the configuration space illustrated by the sphere on the right side of the figure. The three developable surfaces map to the three curves, and they meet at a common point corresponding to contact of the tritangent plane. The endpoints of these curves correspond to the surface normal at the *godrons*. Note that the 2-D stratum of S^2 is not a regular set.

5.3 Capture Regions of Polyhedra

Polyhedra are perhaps the most important class of models of manufactured objects. As discussed above, contact between a point $\mathbf{x} \in \mathcal{H}$ and the supporting plane occurs for configurations $\mathbf{q} \in S^2$ that lie in the normal cone $N_c(\mathbf{x})$ (Clarke 1990). Thus, the configuration space S^2 can be stratified according to the generalized normal. Because the faces of a polyhedron are planar and the edges are linear, the generalized normal of faces and edges do not subtend regions of S^2 as they do for piecewise-smooth curved objects. In particular, each face of the polyhedral hull maps to a single configuration defined by the normal to the face. An edge between two faces maps to an arc of a great circle on the sphere; this can be seen by considering equation (10) and noting that $\mathbf{n}_1$ and $\mathbf{n}_2$ are constant along the edge. The endpoints of these arcs are the surface normals of the two faces incident to the edge. Finally, vertices correspond to regions of the sphere delimited by the image of the edges incident to the vertex. Figure 6.c shows the stratification of the configuration space for the convex hull in Figure 6.b. The vertex at the north pole is the image of the top face while the lines of latitude correspond to the edges surrounding this face. The vertices along the equator are the image of the vertical faces while the edges along the equator correspond to the vertical edges of the hull.

The vertices of $\mathcal{H}$ correspond to 2-D strata on the sphere, the edges define 1-D strata, and the faces lead to 0-D strata. Let us now characterize the critical points of the potential energy function on this stratified set and show how the normal and tangential Morse data are computed.

First, consider the critical points of the potential energy function restricted to the 2-D stratum associated with contact at a vertex $\mathbf{v}$. The potential energy $u(\mathbf{q})$ is given by:

$$u(\mathbf{q}) = (\mathbf{v} - \mathbf{c}) \cdot \mathbf{q} \tag{11}$$

where $\mathbf{q}$ lies in the generalized normal of $\mathbf{v}$. Differentiating (11), the critical points occur when $\mathbf{v} - \mathbf{c}$ is parallel to $\mathbf{q}$ (i.e. when the center of gravity lies above the vertex). Evaluating the Hessian matrix of (11) at the critical points reveals that the Morse index is $\lambda = 2$. Thus from Theorem 2, the tangential Morse data is $(D^2, \partial D^2)$. Since the stratum is two dimensional which equals the dimension of S^2, the normal Morse data is $(D^0, \emptyset)$. Thus, the Morse data characterizing the topological change is simply $(D^2, \partial D^2)$ which is identical to a classical local maximum. Figure 9.a shows a pictorial representation of the Morse data.

Now, consider the one dimensional stratum associated with an edge formed by the intersection of two planar faces whose unit normals are $\mathbf{n}_1$ and $\mathbf{n}_2$. Let the two vertices $\mathbf{v}_1$ and $\mathbf{v}_2$ be the endpoints of the edge. Since the normals are constant along the edge and from (10), the potential energy can expressed as:

$$u(\theta) = (\mathbf{v}_i - \mathbf{c}) \cdot \mathbf{q}(\theta) \tag{12}$$

where the configuration is given by

$$\mathbf{q}(\theta) = \cos\theta \, \mathbf{n}_1 + \frac{\sin\theta}{|(\mathbf{n}_1 \times \mathbf{n}_2) \times \mathbf{n}_1|} (\mathbf{n}_1 \times \mathbf{n}_2) \times \mathbf{n}_1.$$

	Normal Morse Data	Tangential Morse Data	Morse Data
a. 2D Stratum (vertex contact)	$(\bullet , \varnothing)$	$\times \ (\bullet , \bigcirc)$	$= (\bullet , \bigcirc)$
b. 1D stratum (edge contact)	$(\wedge , \bullet\ \bullet)$	$\times \ (\mid , :)$	$= (\ ,\ )$
c.	$(\ , \bullet)$	$\times \ (\mid , :)$	$= (\ ,\ )$
d.	$(\vee , \varnothing)$	$\times \ (\mid , :)$	$= (\ , \ <)$
e. 0D stratum (face contact)	$(\triangledown , \varnothing)$	$\times \ (\bullet , \varnothing)$	$= (\triangledown , \varnothing)$
f.	$(\ , <)$	$\times \ (\bullet , \varnothing)$	$= (\ , <)$
g.	$(\ , \subset)$	$\times \ (\bullet , \varnothing)$	$= (\ , \subset)$
h.	$(\triangle , \frown)$	$\times \ (\bullet , \varnothing)$	$= (\triangle \ \frown)$

Figure 9: A pictorial representation of the tangential Morse data, the normal Morse data, and the Morse data along the 0, 1, and 2 dimensional strata of S^2. The following types of critical points are particularly noteworthy: a. A nonsmooth maximum; d. A nonsmooth saddle; e. A nonsmooth minimum.
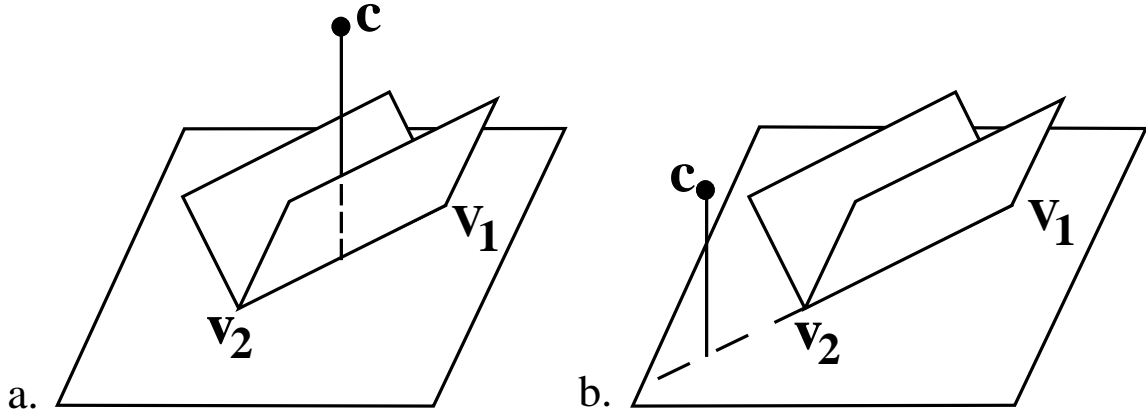
Figure 10: In the critical configuration with the center of gravity **c** above the edge, there are two possible relationships of **c** with respect to the vertices $\mathbf{v}_1$ and $\mathbf{v}_2$. If **c** lies above either $\mathbf{v}_1$ or $\mathbf{v}_2$, $u(\mathbf{q})$ is not a Morse function.

Differentiating (12) with respect to θ, the critical points of $u(\mathbf{q})$ restricted to the 1-D stratum occur when the center of gravity **c** lies directly above or directly below the edge. However, **c** must always lie above the supporting plane as shown in Figure 10; thus, the critical point $\mathbf{q}_e$ must be a local maximum ($\lambda = 1$) of $u(\mathbf{q})$ when restricted to the stratum, and so the tangential Morse data is $(D^1, \partial D^1)$. The normal slice corresponds to a curve (a one dimensional disk) through $\mathbf{q}_e$ which is transverse to $\mathbf{q}(\theta)$. A trajectory along the normal slice corresponds to rolling the object from contact at vertex $\mathbf{v}_1$ to contact along the edge to contact at vertex $\mathbf{v}_2$. Since the normal Morse data is defined by the limiting behavior, the normal Morse data can be represented as piecewise-linear. Furthermore, since the $u(\mathbf{q})$ is assumed to be Morse in the sense of stratified Morse theory, Condition (3) of Section 5.1 implies that the potential energy must be either strictly increasing or strictly decreasing for a trajectory along the normal slice while in contact with either $\mathbf{v}_1$ or $\mathbf{v}_2$. Up to interchanging $\mathbf{v}_1$ and $\mathbf{v}_2$, the normal Morse data can only take the three forms illustrated in Figure 9.b-d.

A further geometric analysis of the normal slice reveals that the situation shown in figure 9.b is impossible. Consider in Figure 10 the relationship between **c** and the edge in the critical configuration. In Fig. 10.a, the potential energy increases when rolling onto either $\mathbf{v}_1$ or $\mathbf{v}_2$. In Fig. 10.b, the potential energy increases when rolling onto $\mathbf{v}_1$ and decreases when rolling onto $\mathbf{v}_2$. Up to interchanging $\mathbf{v}_1$ and $\mathbf{v}_2$ in Fig. 10.b, these are the only two generic situations for an edge contact, and so the normal Morse data shown in Figure 9.b cannot occur. Note that if **c** were to lie directly above vertex $\mathbf{v}_i$ during an edge contact, $u(\mathbf{q})$ would not be a Morse function since $\lim_{\mathbf{q} \to \mathbf{q}_e} \nabla u(\mathbf{q}) = 0$ for $\mathbf{q}$ restricted to the 2-D stratum associated with $\mathbf{v}_i$.

The connectivity of the set $S^2_{\leq u}$ does not change for the critical point type shown in Figure 9.c. However for the critical point shown in Figure 9.d, the connectivity change is like a classical saddle point; two points on the boundary of $S^2_{\leq u}$ are merged at these *nonsmooth saddles*. As with the Type I and Type II saddles of Section 4, a nonsmooth saddle can either join two disjoint components of $S^2_{\leq u}$, or it can introduce a puncture into a single component.

All zero dimensional strata (contact with a face) are critical points of $u(\mathbf{q})$, and the tangential
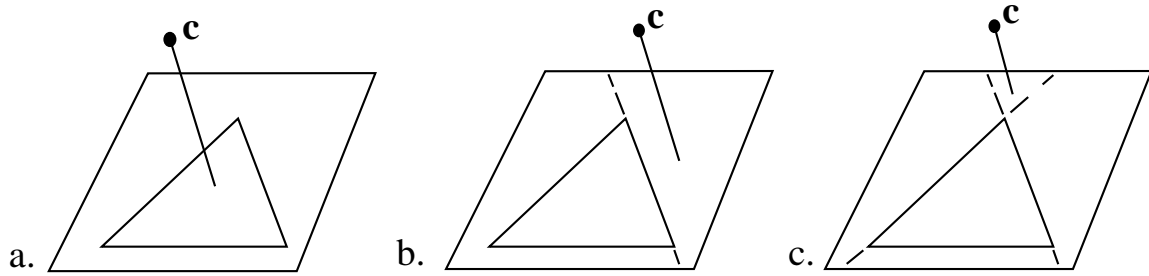
Figure 11: For contact with a triangular face, there are three distinct (generic) relationships between the projection of the center of gravity **c** in the direction of **g** and the edges of the triangle: a. The projection of **c** lies within the triangle; b. The projection of **c** is outside of one edge; c. The projection of **c** is outside of two edges. When **c** lies above an edge or vertex of the triangle, $u(\mathbf{q})$ is not a Morse function.

Morse data is $(D^0, \emptyset)$. The form of the normal Morse data depends on the number of edges surrounding the face. For simplicity of presentation, only triangular faces will be considered here. Since the normal slice is defined locally (i.e., by a small ball around the critical configuration), we can consider a first order approximation of $u(\mathbf{q})$. Also because $u(\mathbf{q})$ is assumed to be Morse, $\nabla u(\mathbf{q})$ must be nonzero along the 1-D and 2-D stratum incident to the critical point. Thus, the normal Morse data can assume four possible forms shown in Figure 9.e-h. However as seen in Figure 11, there are only three qualitatively different relationships between **c** and the triangular face; from these relationships, it can be seen that the Morse data in Figure 9.h is impossible. That is, contact on a face cannot be a local maximum of potential energy. The Morse data shown in Figure 9.e is a *nonsmooth local minimum* and corresponds to the center of gravity lying above the supporting face as illustrated in Figure 11.a. A new region is introduced to $S^2_{\leq u}$ when the corresponding critical value is crossed. The other two critical points shown in Figures 9.f and 9.g respectively correspond to the situations shown in Figures 11.b and 11.c where the center of gravity lies outside one or two of the edges of the triangular face. Crossing one of these critical points does not lead to a connectivity change of $S^2_{\leq u}$. Finally, if **c** lies above an edge or vertex of the face, $u(\mathbf{q})$ is not a Morse function.

5.3.1   Algorithmic and Implementation Details

The algorithm for computing the capture regions of an object with a polyhedral convex hull has the same structure as the one for smooth objects outlined in Section 4.1.1. Here, we detail the differences and show that the computational complexity for computing the capture regions of a convex polyhedron with n faces is $O(n^2)$. For nonconvex polyhedra, the hull can be precomputed.

As discussed above, there are a total of six different types of critical points shown in Figures 9.a, 9.c, 9.d, 9.e, 9.f and 9.g. Of these, only three lead to changes in connectivity of the set $S^2_{\leq u}$: the nonsmooth minimum (Fig. 9.e) introduces a new region, the nonsmooth saddle (Fig. 9.d) leads to a change in connectivity, and the smooth maximum (Fig. 9.a) closes a puncture. Based on the characterization presented above, the relevant critical points can be computed easily and characterized from a CAD model using simple geometric tests. Note that determining the critical points is much simpler than for algebraic surfaces since only linear or quadratic equations are

solved. Because there are $O(n)$ edges and vertices for a convex polyhedron with n faces (Preparata & Shamos 1985) and since there can be at most one critical configuration per face, edge or vertex, there are only $O(n)$ critical points.

The two equipotential contours through a nonsmooth saddle point are easy characterized as well. In particular, they are given by a sequence of circular arcs whose endpoints lie on a one dimensional stratum. Each arc corresponds to rolling about a vertex while the center of gravity maintains constant height above the supporting plane. While the contours of constant potential energy u_b were defined implicitly for algebraic surfaces and had to be traced numerically in Section 4.1.4, they are given explicitly for contact with a vertex $\mathbf{v}$ as:

$$\mathbf{q}(t) = \cos t\, \mathbf{i} + \sin t\, \mathbf{j} + \mathbf{k}, \quad t \in [t_{min}, t_{max}] \tag{13}$$

where $\mathbf{i}, \mathbf{j}$ and $\mathbf{k}$ are orthogonal, $|\mathbf{i}| = |\mathbf{j}| = \sqrt{1 - \left(\frac{u_b}{|\mathbf{v}-\mathbf{c}|}\right)^2}$ and $\mathbf{k} = \frac{u_b}{|\mathbf{v}-\mathbf{c}|}(\mathbf{v} - \mathbf{c})$. The limits of the interval $[t_{min}, t_{max}]$ correspond to the configurations where one of the edges incident to $\mathbf{v}$ contacts the supporting plane. This configuration can be computed by equating (13) with the edge equation (10). Starting at a saddle point, a sequence of arcs are found by marching from vertex to vertex until an arc returns to the original saddle point. As shown in the examples in Figures 12 and 13, both equipotential contours are tangent to the 1D edge strata at the saddle points. Because the contour equations are given explicitly, tangency does not lead to numerical difficulties. It is easy to show that there are at most two intersections between an equipotential contour and the stratum corresponding to an edge. Since an equipotential contour may cross all of the 1-D strata, an equipotential contour may be composed of at most $O(n)$ circular arcs which can be computed in $O(n)$ time. Figure 13 shows an object whose equipotential contours are composed of many arcs.

After computing the two equipotential contours through a saddle point, the next step of the algorithm is to determine if one of the two loops surrounds a minimum on the `region-list`. For a smooth surface, this was accomplished by integrating the first order system given by (8). For polyhedra, graph search can be used. On S^2, the 0-D strata (faces) are connected by 1-D strata (the edges), and this defines a graph with the faces as nodes and the edges as vertices. Elimination of the edges that intersect the equipotential contour will partition this graph into two disjoint subgraphs; one of the subgraphs contains faces with lower potential energy than the nonsmooth saddle point. This subgraph can be searched for a minimum (face) on the `region-list` starting at a face within the subgraph which is adjacent to the edge containing the saddle. Since the graph has $O(n)$ nodes and edges, it can be searched in $O(n)$ time. Consequently, the total running time and maximum size of the capture regions is $O(n^2)$ since there are $O(n)$ saddle points and the equipotential contour through each saddle point can cross at most $O(n)$ edges.

5.3.2 Some Examples

The algorithm for computing the capture regions of polyhedral objects has been completely implemented in Common Lisp, and we will now consider two examples. The capture regions for both examples are computed in under three seconds.

Figure 6.a shows a model of an insulator cap while Figure 6.b shows its convex hull. The configuration space is stratified according to the generalized normal of the hull and shown in Figure 6.c. Note that because the hull is a generalized cylinder, the top and bottom faces correspond to the poles of the sphere. In spherical coordinates, the poles are the entire top and bottom edges
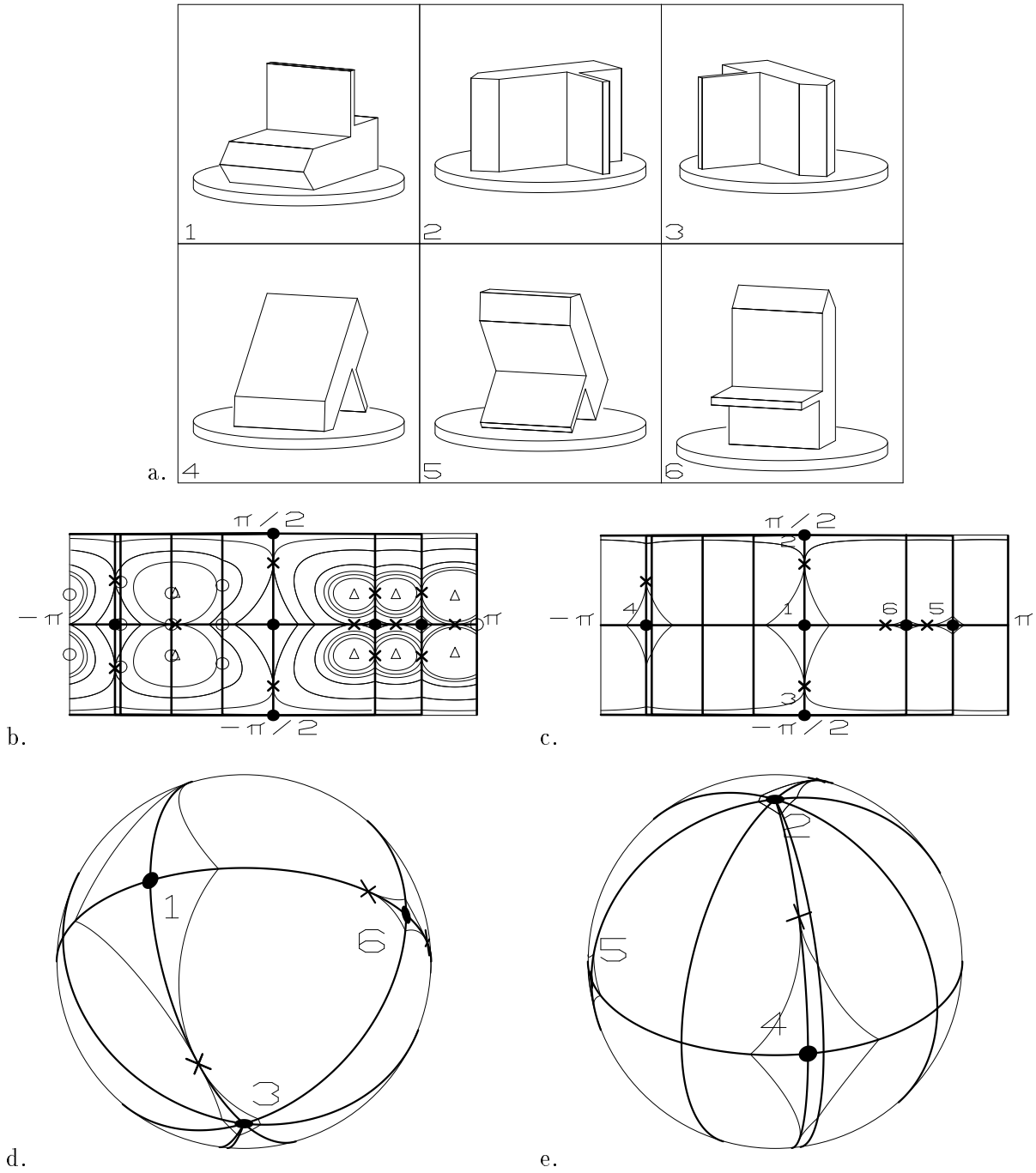
Figure 12: The capture region of the insulator cap shown in Figure 6: a. The six stable poses of the insulator cap ordered by increasing potential energy. b. The critical points and all equipotential contours through the saddles in spherical coordinates. Solid circles indicate nonsmooth minima, triangles indicate smooth maxima, X's indicate nonsmooth saddle points, and the empty circles are other types of nonsmooth critical points. In this and subsequent drawings, the thicker curves represent one dimensional strata of the configuration space while the thinner lines are equipotential contours; c. For each stable pose numbered according to Figure 12.a, the capture regions are drawn in spherical coordinates; d, e. Antipodal views of the capture regions drawn on the sphere.

Capture Region	Energy of Minimum	Energy of Saddle
1	35.54	43.55
2	42.41	43.55
3	44.90	45.18
4	44.95	55.64
5	45.53	50.83
6	45.75	50.58
7	49.17	50.45
8	53.05	53.17
9	54.85	55.16
10	55.05	55.06

Table 1: For each capture region of the clamp in Figure 13, this table shows the relative potential energy of the corresponding minima and saddle points.

of the drawing; the edges surrounding these faces become lines of longitude (meridians), and the vertical edges map to the equator. With $c = (.02, -.2, 0.0)$, there are 38 critical points shown in Figure 12.b of which six are nonsmooth minima (stable faces), twelve are nonsmooth saddles, and eight are smooth maxima. This agrees with the Euler characteristic. Figure 12.a shows the six stable configuration numbered by increasing potential energy. Figure 12.c shows the capture regions. Note that while the part's hull has ten faces, only six are stable. Figures 12.d,e show the capture regions drawn on the sphere which does not distort their size as drastically. As seen in Figures 12.c,e, Capture Region 4 contains an unstable face; consequently, if the part starts at rest in contact with that face, it will topple onto the adjacent stable face.

Finally, consider the chemistry clamp shown in Figure 13.a and the convex hull of a polyhedral approximation drawn in Figure 13.b. This hull contains 33 faces, 33 edges and 64 vertices. Figure 13.c shows the 10 local minima (stable poses) and 12 local maxima along with the equipotential contours through the 20 nonsmooth saddle points. Note that the forty closed equipotential contours cross the 1-D strata many times and are composed of many circular arcs. At the 41 other critical points, the connectivity of the capture regions does not change. Figures 13.d-f show the ten capture regions drawn in both spherical coordinates and on the sphere. Observe that only 10 of the 33 faces are stable. Of the ten stable faces, only four capture regions (numbers 1, 4, 5 and 6) cover a significant area of the sphere. It would seem that the six smaller regions might only be marginally stable in the sense that the addition of a small amount of kinetic energy would allow the object to move out of the capture region. As shown in Table 1, the relative potential energy of the local minimum and corresponding saddle point is much greater for the four larger regions.
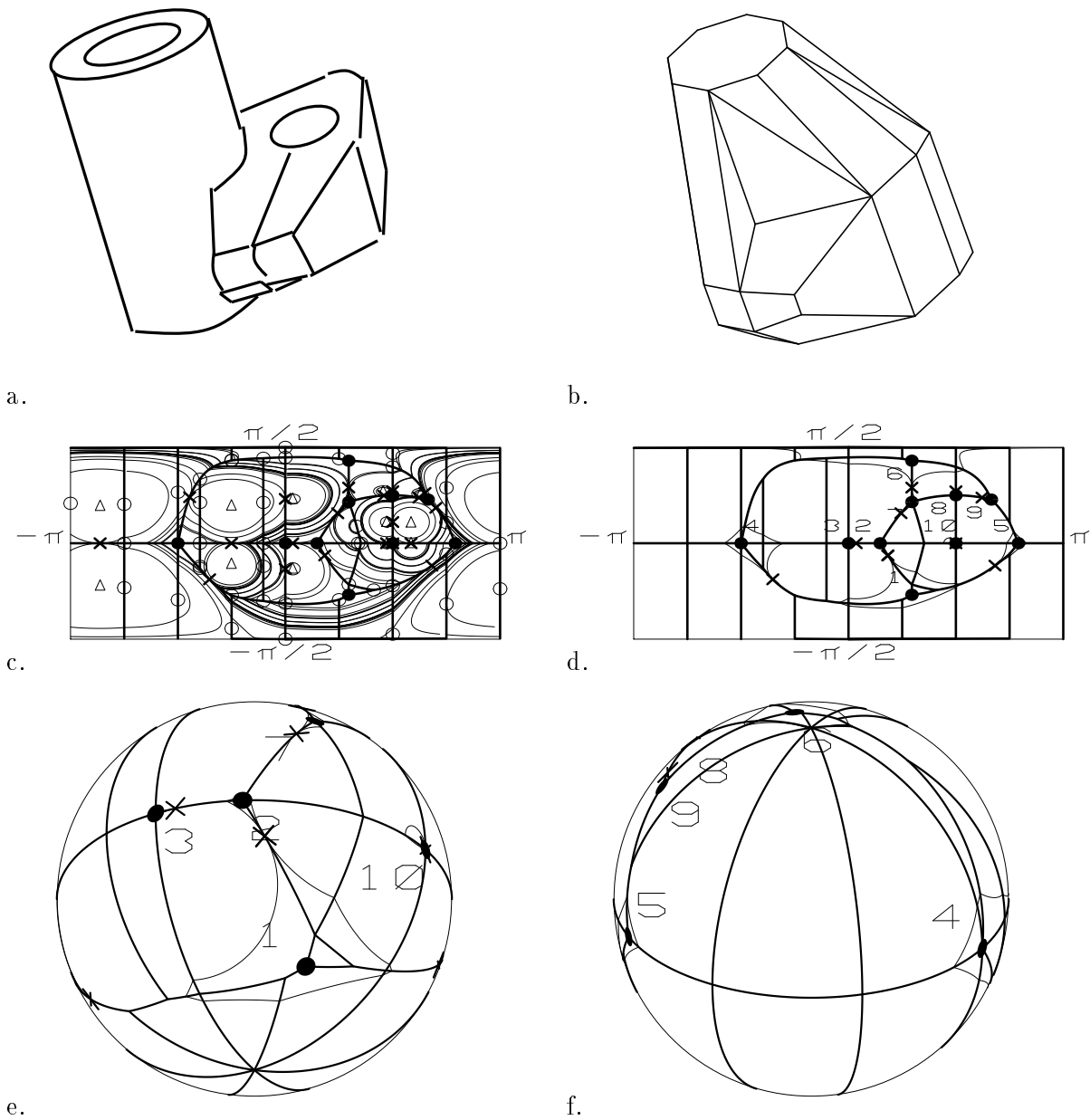
26

a.

b.

c.

d.

e.

f.

Figure 13: The capture regions for a chemistry clamp: a. A line drawing of the clamp; b. The convex hull of a polyhedral approximation with hidden lines removed; c. The equipotential contours through all 20 nonsmooth saddles. d. The capture regions in spherical coordinates; e, f. Antipodal views of the capture regions drawn on the sphere.

5.4 Capture Regions of parts with C^1 Hulls

We now consider the capture regions of smooth parts with concavities. As discussed in Section 5.2, the convex hull $\mathcal{H}$ of such a part is C^1. The hull's surface is continuous and has a continuous tangent plane; however, higher order derivatives may be discontinuous. The configuration space of the part in contact with a support plane is stratified according the generalized normal. We first develop a catalogue of the types of critical points of $u(\mathbf{q})$. Some of these were considered earlier, and additional ones will be presented in Figures 15 and 16.

The two dimensional strata of S^2 correspond to points of $\mathcal{H}$ that also lie on the original smooth part as shown in Figure 7.a. Consequently, for $\mathbf{q}$ restricted to the 2-D strata, the critical points of $u(\mathbf{q})$ are the same as for smooth parts with C^3 hulls. As in Section 4, they can be classified as smooth minima, saddles or maxima.

As discussed in Section 5.2 and shown in Figure 7.b, the one dimensional strata of S^2 correspond to contact with the supporting plane along a bitangent developable surface of $\mathcal{H}$. We now consider the critical points of $u(\mathbf{q})$ for $\mathbf{q}$ restricted to a 1-D stratum. Let a ruled surface be parameterized by $\mathbf{x}(t,v) = \boldsymbol{\alpha}(t) + v\mathbf{w}(t)$ where $\boldsymbol{\alpha}(t)$ and $\mathbf{w}(t)$ are vector valued functions. The ruled surface is said to be developable when $\mathbf{w} \times \dot{\mathbf{w}} \cdot \boldsymbol{\alpha} = 0$ in which case the Gaussian curvature is identically zero (do Carmo 1976). Furthermore, it is easy to show that the surface normal $\mathbf{n}$ is constant along a ruling and can be expressed as a function of t only.

$$\mathbf{n}(t) = \dot{\boldsymbol{\alpha}}(t) \times \mathbf{w}(t)$$

The potential energy for contact along the developable surface can be written as

$$u(t) = (\boldsymbol{\alpha}(t) - \mathbf{c}) \cdot \hat{\mathbf{n}}(t)$$

where the unit normal is $\hat{\mathbf{n}} = \frac{1}{|\mathbf{n}|}\mathbf{n}$. Differentiating $u(t)$, the critical points are found by solving the following for t:

$$(\boldsymbol{\alpha} - \mathbf{c}) \cdot \dot{\hat{\mathbf{n}}} = 0 \tag{14}$$

It is easy to show that this condition is equivalent to the center of gravity being above the developable line that is in contact with the support plane. The critical point may either be a local maximum or minimum of $u(t)$, and so the tangential Morse data along this 1D stratum can be depicted as $(\mid, :)$ or $(\mid, \emptyset)$.

To determine the normal Morse data, we study $u(\mathbf{q})$ restricted to the normal slice (a curve that intersects the 1-D stratum transversally at the critical point). Rather than expressing the potential energy as a function of $\mathbf{q}$, it will more intuitive to define it on the hull. Consider the plane formed by $\mathbf{c}$ and the supporting developable in the critical configuration. As depicted in Figure 14, the intersection of this plane with $\mathcal{H}$ defines a curve that bends toward $\mathbf{c}$ in the neighborhood of the developable. Note that the curve's tangent is continuous at the end points of the developable. Up to an interchange of $\mathbf{v}_1$ and $\mathbf{v}_2$, the center of gravity can assume two qualitatively different locations as shown in figure 14.a and 14.b. Because $u(\mathbf{q})$ is assumed to be Morse, $\mathbf{c}$ cannot lie above $\mathbf{v}_1$ or $\mathbf{v}_2$ since ∇u would vanish, and this would violate the third requirement of a Morse function given in Section 5.1. In the case of Figure 14.a which is similar that shown in Figure 10.a, the potential increases as the point of contact rolls past either $\mathbf{v}_1$ or $\mathbf{v}_2$ since the length of $\mathbf{v_i} - \mathbf{c}$ is greater than the minimum distance from $\mathbf{c}$ to the developable. Thus, the critical point is a nonsmooth local minimum in the normal slice and has normal Morse data as in Figures 15.b or 15.d.
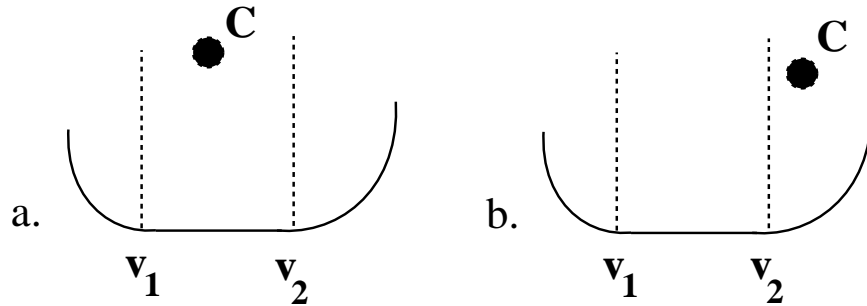
Figure 14: Within a plane defined by the center of gravity **c** and the critical developable, there are two possible relationships between **c** and the endpoints of the developable.

On the other hand, consider the situation shown in figure 14.b; when the object rolls along $\mathbf{v_1}$, u will increase as in Fig. 14.a. When the object rolls along $\mathbf{v_2}$, it is not obvious whether u will increase or decrease, so we will consider this case in more detail. Let the planar intersection curve $\mathbf{x}(s)$ be parameterized by arc length s with s increasing from left to right. The curve normal is upward pointing, and the curvature $k(s)$ is non-negative. We can write the potential energy as:

$$u(s) = (\mathbf{x}(s) - \mathbf{c}) \cdot (-\mathbf{n}(s))$$

For a plane curve we have that $\dot{\mathbf{n}}(s) = -k(s)\mathbf{t}(s)$ from the Frenet equations (do Carmo 1976), and so

$$\frac{du}{ds} = (\mathbf{c} - \mathbf{x}) \cdot \dot{\mathbf{n}}(s) = k(s)(\mathbf{x} - \mathbf{c}) \cdot \mathbf{t}(s).$$

Considering the limit as $\mathbf{x}(s)$ approaches $\mathbf{v_2}$ from the right; we have that $k(s) > 0$ and that $(\mathbf{x} - \mathbf{c}) \cdot \mathbf{t}(s) < 0$. Thus, $\frac{du}{ds}$ is negative, and so $u(s)$ is monotonic in s; consequently, the normal Morse data has the same form as shown Figures 15.a and 15.c which is identical to the form in Figure 9.c

In summary, the tangential Morse data can assume two forms (smooth minimum or maximum), and the normal Morse data can either be a nonsmooth minimum or is monotonic. This leads to four possible forms for the local Morse data shown in Figure 15. The connectivity changes to $S^2_{\leq u}$ follow: the critical point shown in Figure 15.d is a nonsmooth local minimum and introduces a new component; this is similar to the stable configuration of a rocking horse. The critical point type shown in Figure 15.b is a nonsmooth saddle which joins together two components of $S^2_{\leq u}$. The other two critical point types do not change the connectivity of $S^2_{\leq u}$.

Recall from Section 5.1 that all zero dimensional strata are critical points and from Section 5.2 that there are two types of 0-D strata on S^2; they correspond to the surface normal at the endpoint of a bitangent developable (*godron*) shown in figure 7.g or to the Gaussian image of the tritangent planes where the image of three developables meet on S^2 (e.g. Figure 7.c). For both types of zero dimensional strata, the tangential Morse data is the identity ($\cdot$, $\emptyset$), and so the Morse data is given by the normal Morse data.

Consider first the *godrons*. Since the tangent plane of the graph $(\mathbf{q}, u(\mathbf{q}))$ is discontinuous across the Gaussian image of the bitangent developable, $(\mathbf{q}, u(\mathbf{q}))$ has a crease that ends at the critical point. By the assumption that $u(\mathbf{q})$ is Morse, the limit of $\nabla u(\mathbf{q})$ as $\mathbf{q}$ approaches the critical point
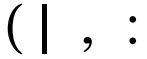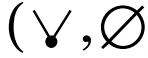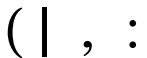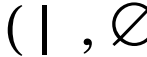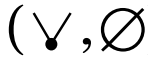
Normal Morse Data	Tangential Morse Data	Morse Data
a. $(\,\cdot\,,\;\cdot\,) \times (\;|\;,\;:) = (\;\;,\;\smile)$		
b. $(\vee,\varnothing) \times (\;|\;,\;:) = (\;\;,\;<)$		
c. $(\,\cdot\,,\;\cdot\,) \times (\;|\;,\varnothing) = (\;\;,\;\frown)$		
d. $(\vee,\varnothing) \times (\;|\;,\varnothing) = (\;\;,\varnothing)$		

Figure 15: The Morse data for critical points on a 1-D stratum of S^2 for an object with a C^1 convex hull.

$$\mathbf{a.}\;\left(\;\;,\;<\right) \qquad \mathbf{b.}\;\left(\;\;,\;\subset\right)$$

Figure 16: For an object with a C^1 convex hull, the end points of the bitangent developables (the *godrons*) define the 0-D strata, and the Morse data can assume two forms.

must be nonzero when $\mathbf{q}$ is restricted to either the 1-D or 2-D strata. So, the normal Morse data can take on the two forms shown in figure 16. Neither of these two types of critical points leads to a change in the connectivity of $S^2_{\leq u}$, and so *godrons* do not play a role in defining capture regions.

Analysis of the zero dimensional strata corresponding to contact with a tritangent planes is completely analogous to the 0-D strata for polyhedra with triangular faces described using Figure 11, and the Morse data will be as in Figure 9.e–g. When the projection of $\mathbf{c}$ onto the tritangent plane lies within the triangle defined by the three contact points, the critical point is a local minimum of $u(\mathbf{q})$ as in Figure 9.e, and a new region $S^2_{\leq u}$ is created.

In summary, there are three types of local minima which introduce new regions into $S^2_{\leq u}$: the smooth minimum on a 2-D stratum, the nonsmooth minimum on a 1-D stratum shown in Figure 15.d, and the nonsmooth minimum corresponding to contact of the tritangent plane shown in Figure 9.e. There are two types of saddle points which either join two connected components of $S^2_{\leq u}$ or introduce a puncture into one component: the smooth saddle on a 2D stratum and the nonsmooth saddle on a 1-D stratum illustrated in Figure 15.b. The algorithm outlined in Section 4.1.1 for computing capture regions can be extended to objects with this class of hulls using

the critical points described above. The only complications that arise are tracing the equipotential contours and following the gradient $\nabla u(\mathbf{q})$ since the trajectory $\mathbf{q}(t)$ may cross a 1-D strata where $u(\mathbf{q})$ is not smooth. However, it is a simple matter to consider the limits of $\nabla u(\mathbf{q})$ as $\mathbf{q}$ approaches the 1-D stratum during these operations. The algorithm for constructing the capture regions of this class of hulls has not yet been implemented.

6   Conclusions

This paper analyzed the problem of computing capture regions of a 3-D object under dissipative dynamics using the tools of stratified Morse theory. An implemented algorithm demonstrates the computability of these regions for polyhedral parts and algebraic surfaces with a C^3 convex hull. The approach can be extended to handle objects with a piecewise-smooth hull, and this includes most objects modelled using CAD systems. The two things that are lacking for this class of objects are a complete catalogue of convex hull points and an implemented algorithm for actually constructing the hull; however, see (Hung & Ierardi 1994) for recent progress. We noted in Section 2 that there is a hierarchy of capture regions; the presented algorithms can be easily extended to construct this containment graph. The presented approach only applies to parts whose potential energy functions are Morse. It would be interesting to classify the types of non-generic critical points that might occur for symmetric objects.

One assumption in this paper has been that the object remains in contact with the support plane (i.e. it does not bounce). Stratified Morse theory can also be used to show that the capture regions hold even under bouncing. Define the potential energy over both orientation and the height (i.e. $u : \mathbb{R} \times S^2 \to \mathbb{R}$) as given by $\mathbf{r}_3$ and $\mathbf{t}_z$ in (1). From Theorem 3, we note that the topology only changes at critical points. Since u is monotonic in the height of $\mathbf{c}$, there are no critical points on the 3-D strata of $S^2 \times \mathbb{R}$. Thus, the critical points given in this paper will be the critical points when the object is free to break contact with the support plane. Thus, the method holds even when the object bounces.

Other applications of the capture region idea which would take advantage of stratified Morse theory are fixturing and grasping. Conditions for an object's pose to be stable in a fixture were addressed in (Brost 1991b) for polygons in 2-D and more generally in (Mason et al. 1995). Brost also presented methods for computing capture regions for a polygonal object and a polygonal fixture. To extend this to 3-D objects (possibly with curved surfaces), the five dimensional contact configuration space should be partitioned, and stratified Morse theory can be used to develop a catalogue of critical points. Now, consider grasping an object with two or more fingers. For some stable grasps, if the fingers contact the object near the stable grasp, the object will move in a manner whereby the fingers converge to this grasp. The set of initial contact configurations from which the object will converge to the desired grasp can be determined using the approach presented in this paper when the control law for the fingers leads to dissipative dynamics.

Finally, in recent work with K. Goldberg and A. Rao, we have used capture regions within a part feeding application based on an arm with only four active degrees of freedom plus a passive pivoting axis between the parallel jaws of a gripper (Carlisle et al. 1994; Rao et al. 1995). The idea is to grasp a part with 2 hard finger contacts such that it pivots, under gravity, into a desired orientation when lifted and replaced on the table. Given a polyhedral part shape, coefficient of friction and a pair of stable configurations as input, an algorithm was presented for finding pairs

of grasp points that cause the part to pivot from one stable configuration to the other. For some pairs of stable configurations, such a grasp may not exist; however, it may be possible to achieve the desired final pose using a sequence of pivoting and regrasping operations. Alternatively, the desired final configuration may also be achieved by simply pivoting the part to a configuration within a capture region and allowing gravity to do the rest. While the position and orientation of the part in the support plane cannot be predicted, there are numerous reorientation methods using fences (Brokowski, Peshkin & Goldberg 1993), a tilting table (Erdmann et al. 1993) or a manipulator (Goldberg 1993).

Acknowledgments

References

Arnol'd, V. (1984), *Catastrophe Theory*, Springer-Verlag, Heidelberg.

Banchoff, T., Gaffney, T. & McCrory, C. (1982), *Cusps of Gauss Mappings*, Pitman, Boston.

Boothroyd, G. & Ho, C. (1977), 'Natural resting aspects of parts for automatic handling', *ASME Journal of Engineering for Industry* **99**, 314–317.

Boothroyd, G., Redford, A., Poli, C. & Murch, L. (1972), 'Statistical distributions of natural resting aspects of parts for automatic handling', *SME Manufacturing Engineering Transactions* **1**(72), 93–105.

Brokowski, M., Peshkin, M. & Goldberg, K. (1993), Curved fences for part alignment, *in* 'IEEE Conf. on Robotics and Automation', pp. 467–473.

Brost, R. C. (1991*a*), Analysis and Planning of Planar Manipulation Tasks, PhD thesis, Carnegie Mellon.

Brost, R. C. (1991*b*), Computing possible rest configurations of two interacting polygons, *in* 'IEEE Conf. on Robotics and Automation', pp. 686–693.

Brost, R. C. (1992), Dynamic analysis of planar manipulation tasks, *in* 'IEEE Conf. on Robotics and Automation', pp. 2247–2254.

Canny, J. (1988), *The Complexity of Robot Motion Planning*, MIT Press.

Carlisle, B., Goldberg, K., Rao, A. & Wiegley, J. (1994), A pivoting gripper for feeding industrial parts, *in* 'IEEE Conf. on Robotics and Automation', pp. 1650–1655.

Chiang, H., Hirsch, M. & Wu, F. (1988), 'Stability regions of nonlinear autonomous dynamical systems', *IEEE Trans. on Automatic Control* **33**, 16–27.

Clarke, J. H. (1990), *Optimization and Nonsmooth Analysis*, SIAM Press, Philadelphia.

Collins, G. E. (1975), *Quantifier Elimination for Real Closed Fields by Cylindrical Algebraic Decomposition*, Vol. 33, Springer-Verlag, New York.

do Carmo, M. (1976), *Differential Geometry of Curves and Surfaces*, Prentice-Hall, Englewood Cliffs, N.J.

Donald, B. (1988), 'A geometric approach to error detection and recovery for robot motion planning with uncertainty', *Artificial Intelligence* **37**, 223–271.

Erdmann, M. (1986), 'Using backprojections for fine motion planning with uncertainty', *Int. J. Robot. Res.* **5**(1), 19–45.

Erdmann, M. A., Mason, M. T. & Vaněček, G. (1993), 'Mechanical parts orienting: The case of a polyhedron on a table', *Algorithmica*.

Genesio, R., Tartaglia, M. & Vicino, A. (1985), 'On the estimation of asymptotic stability regions: State of the art and new proposals', *IEEE Trans. Automatic Control* **30**(8), 747–755.

Goldberg, K. (1993), 'Orienting polygonal parts without sensors', *Algorithmica* **10**(2), 201–225.

Goresky, M. & Macpherson, R. (1980), *Stratified Morse Theory*, Springer-Verlag, New York.

Guillemin, V. & Pollack, A. (1974), *Differential Topology*, Prentice-Hall, Englewood Cliffs.

Hung, C.-K. & Ierardi, D. (1994), Constructing convex hulls of piecewise smooth objects, Technical Report USC-CS-94-583, University of Southern California.

Koditschek, D. E. (1991), 'The control of natural motion in mechanical systems', *ASME J. of Dynamic Systems* **113**(4), 547–551.

Koenderink, J. J. (1990), *Solid Shape*, MIT Press, Cambridge, MA.

Kriegman, D. (1994), Let them fall where they may: Computing capture regions of curved 3D objects, *in* 'IEEE Conf. on Robotics and Automation', pp. 595–601.

Kriegman, D. & Ponce, J. (1991), A new curve tracing algorithm and some application, *in* P. J. Laurent, A. L. Méhauté & L. L. Schumaker, eds, 'Curves and Surfaces', Academic Press, pp. 267–170.

Kriegman, D. J. (1992), 'Computing stable poses of piecewise smooth objects', *CVGIP: Image Understanding* **55**(2), 109–118.

Latombe, J.-C. (1991), *Robot Motion Planning*, Kluwer Academic Publishers, Boston.

Lozano-Perez, T., Jones, J., Mazer, E. & O'Donnell, P. (1992), *HANDEY-A Robot Task Planner*, MIT Press, Cambridge.

Lozano-Pérez, T., Mason, M. T. & Taylor, R. H. (1982), 'Automatic synthesis of fine-motion strategies for robots', *Int. J. Robot. Res.* **3**(1), 3–24.

Mason, R., Rimon, E. & Burdick, J. (1995), The stability of heavy objects with multiple contacts, *in* 'IEEE Conf. on Robotics and Automation'.

Milnor, J. (1963), *Morse Theory*, Princeton University Press, Princeton, NJ.

Morgan, A. (1987), *Solving Polynomial Systems using Continuation for Engineering and Scientific Problems*, Prentice Hall, Englewood Cliffs.

Murase, H. & Nayar, S. (1994), 'Illumination planning for object recognition using parametric eigenspaces', *IEEE Trans. Pattern Anal. Mach. Intelligence* **16**(12), 1219–1227.

Ngoi, B., Lim, L. & Lee, S. (1995), 'Analyzing the probabilities of natural resting for a component with a virtual resting face', *SME J. of Engineering for Industry*. In press.

Peshkin, M. & Sanderson, A. (1989), 'Minimization of energy in quasi-static manipulation', *IEEE Trans. on Robotics and Automation* **5**(1), 53–60.

Preparata, F. P. & Shamos, M. I. (1985), *Computational Geometry: An Introduction*, Springer-Verlag, New York.

Rao, A., Kriegman, D. & Goldberg, K. (1995), Complete algorithms for reorienting polyhedral parts using a pivoting gripper, *in* 'IEEE Conf. on Robotics and Automation', pp. 2242–2248.

Rimon, E. & Canny, J. (1994), Construction of c-space roadmaps from local sensory data: What should the sensors look for?, *in* 'IEEE Conf. on Robotics and Automation', pp. 117–123.

Rimon, E. & Koditschek, D. E. (1992), 'Exact robot navigation using artificial potential functions', *IEEE Trans. on Robotics and Automation* **8**(5), 501–518.

Sedykh, V. (1977), 'Singularities of the convex hull of a curve in $\mathbb{R}^3$', *Functional Analysis and Applications* **11**(1), 72–73.

Sedykh, V. (1986), 'Structure of the convex hull of a space curve', *J. of Soviet Mathematics* **33**(1), 1140–53.

Tournassoud, P., Lozano-Perez, T. & Mazer, E. (1987), Regrasping, *in* 'IEEE Conf. on Robotics and Automation', pp. 1924–28.

Whitney, H. (1957), 'Elementary structure of real algebraic variaties', *Annals of Mathematics* **66**(3), 545–556.

Wiegley, J., Rao, A. & Goldberg, K. (1992), Computing a statistical distribution of stable poses of a polyhedron, *in* 'Allerton Conf. on Communications, Control and Computing'.

Zakalyukin, V. (1978), 'Singularities of convex hulls of smooth manifolds', *Functional Analysis and Applications* **11**(1), 225–227.